AGU PUBLICATIONS

Geochemistry, Geophysics, Geosystems

RESEARCH ARTICLE
10.1002/2017GC007238

Special Section:
Carbon Degassing Through Volcanoes and Active Tectonic Regions

The Magmatic Gas Signature of Pacaya Volcano, With Implications for the Volcanic CO_2 Flux From Guatemala

A. Battaglia[1], M. Bitetto[1], A. Aiuppa[1,2], A.L. Rizzo[2], G. Chigna[3], I. M. Watson[4], R. D'Aleo[1], F. J. Juárez Cacao[3], and M. J. de Moor[5]

[1]Dipartimento DiSTeM, Università di Palermo, Palermo, Italy, [2]Istituto Nazionale di Geofisica e Vulcanologia, Palermo, Italy, [3]INSIVUMEH, Ciudad de Guatemala, Guatemala, Central America, [4]School of Earth Sciences, University of Bristol, Bristol, UK, [5]OVSICORI, UNA, Heredia, Costa Rica, Central America

Abstract Pacaya volcano in Guatemala is one of the most active volcanoes of the Central American Volcanic Arc (CAVA). However, its magmatic gas signature and volatile output have received little attention to date. Here, we present novel volcanic gas information from in-situ (Multi-GAS) and remote (UV camera) plume observations in January 2016. We find in-plume H_2O/SO_2 and CO_2/SO_2 ratios of 2-20 and 0.6-10.5, and an end-member magmatic gas signature of 80.5 mol. % H_2O, 10.4 mol. % CO_2, and 9.0 mol. % SO_2. The SO_2 flux is evaluated at 885 ± 550 tons/d. This, combined with co-acquired volcanic plume composition, leads to H_2O and CO_2 fluxes of 2,230 ± 1,390 and 700 ± 440, and a total volatile flux of ~3,800 tons/d. We use these results in tandem with previous SO_2 flux budgets for Fuego and Santiaguito to estimate the total volcanic CO_2 flux from Guatemala at ~1,160 ± 600 tons/day. This calculation is based upon CO_2/total S (S_t) ratios for Fuego (1.5 ± 0.75) and Santiaguito (1.4 ± 0.75) inferred from a gas (CO_2/S_t ratio) versus trace-element (Ba/La ratio) CAVA relationship. The H_2O-poor and low CO_2/S_t ratio (~1.0-1.5) signature of Pacaya gas suggests dominant mantle-wedge derivation of the emitted volatiles. This is consistent with $^3He/^4He$ ratios in olivine hosted fluid inclusions (FIs), which range between 8.4 and 9.0 Ra (being Ra the atmospheric $^3He/^4He$ ratio) at the upper limit of MORB range (8 ± 1 Ra). These values are the highest ever measured in CAVA and among the highest ever recorded in arc volcanoes worldwide, indicating negligible ^4He contributions from the crust/slab.

Key Points:
- We present the first volcanic gas compositional time-series and noble gas compositions of olivine-hosted FIs from Pacaya (Guatemala)
- We identify the magmatic gas signature and the Total Volatile Flux budget for one of the most active CAVA volcanoes for the first time
- Our results contribute novel information on the total volcanic CO_2 budget from Guatemalan volcanoes

Supporting Information:
- Supporting Information S1
- Table S1
- Table S2
- Table S3
- Table S4

Correspondence to:
A. Battaglia,
angelo.battaglia03@unipa.it

Citation:
Battaglia, A., Bitetto, M., Aiuppa, A., Rizzo, A.L., Chigna, G., Watson, I. M., et al. (2018). The magmatic gas signature of Pacaya Volcano, with implications for the volcanic CO_2 flux from Guatemala. *Geochemistry, Geophysics, Geosystems*, *19*, 667–692. https://doi.org/10.1002/2017GC007238

Received 14 SEP 2017
Accepted 30 JAN 2018
Accepted article online 5 FEB 2018
Published online 10 MAR 2018

1. Introduction

After nearly 200 years of dormancy, Pacaya volcano in southern Guatemala (Figures 1 and 2) entered a phase of renewed volcanic activity in 1961 (Rose et al., 2013). Since then, open-vent volcanic activity has persisted at Pacaya, oscillating through periods of mild intra-crateric activity at the Mackenney cone and phases of more intense explosive (strombolian to lava fountaining) and effusive activity (Matías Gómez et al., 2012; Rose et al., 2013). This nearly continuous activity has led to eruption of ≈0.2 km^3 of basaltic magma (Rose et al., 2013), thought to have originated from de-compressional melting of a slightly metasomatized (by slab fluids/melts) mantle wedge (Cameron et al., 2003; Walker et al., 2003). Open-vent degassing activity at Pacaya during 1961-present has also produced sustained emission of magmatic volatiles into the atmosphere (Rodríguez et al., 2004).

When considered against emissions from nearby Fuego and Santiaguito volcanoes (Figure 1), Pacaya dominates the present-day Guatemalan contribution to the Central American Volcanic Arc (CAVA) gas budget (Hilton et al., 2002; Mather et al., 2006; Rodríguez et al., 2004). Pacaya gas emissions are also likely to have been significant over the past several millennia, during which similar eruptive episodes, each lasting centuries, have occurred (Bardintzeff & Daniel, 1992; Conway et al., 1992; Eggers, 1971).

In spite of the above, relatively little attention has been paid in characterizing magmatic degassing and gas signature at Pacaya. While magmatic gas compositions and fluxes are relatively well studied for other top gas CAVA emitters, such as Turrialba in Costa Rica (Aiuppa et al., 2014; Conde et al., 2014; de Moor et al., 2016, 2017; Di Piazza et al., 2015; Moussallam et al., 2014) and Masaya in Nicaragua (Burton et al., 2000; de Moor et al., 2017; Martin et al., 2010), volcanic gas data are available for only two Pacaya fumaroles sampled in the early 1990s (Goff et al., 2000). The fumaroles sampled by Goff et al. (2000), however, were relatively

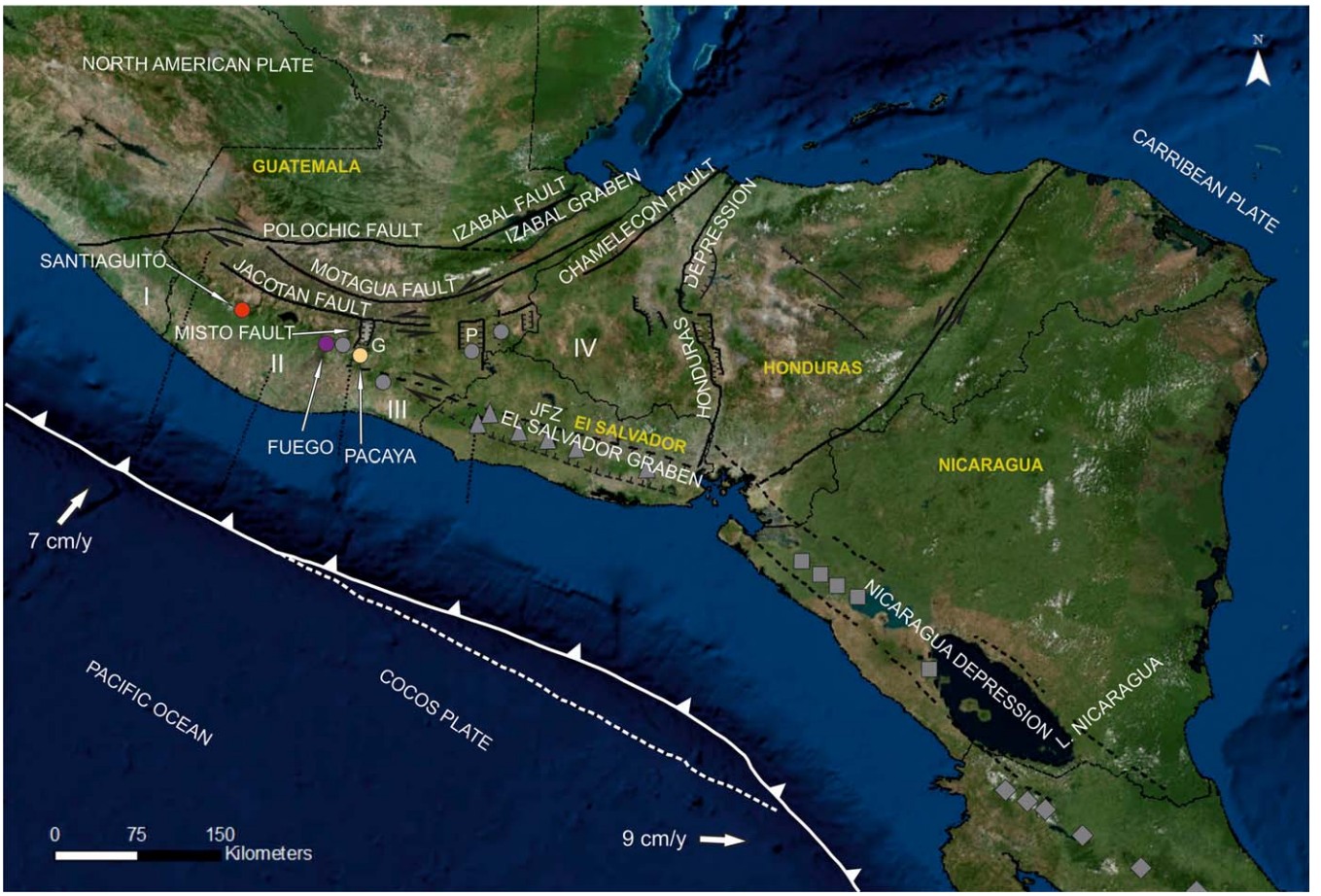

Figure 1. Morphotectonic sketch of Central America, showing location of the active volcanic systems discussed in the text. Red, purple and yellow circles indicate Santiaguito, Fuego and Pacaya volcanoes, respectively. Grey symbols indicate position of other key CAVA volcanoes. Circles: Guatemalan volcanoes; triangles: El Salvador volcanoes; squares: Nicaraguan volcanoes; rhombus: Costa Rica volcanoes. Symbols I, II, III, IV identify the morphotectonic zones described in Burkart and Self (1985). P= Ipala graben; G= Guatemala graben; JFZ= Jalpatagua fault zone.

low in temperature (84.5 and 342°C), implying a non-negligible role of secondary processes (e.g., scrubbing of magmatic volatiles by hydrothermal reactions (Aiuppa et al., 2014, 2017). According to the authors, the $\delta^{13}C$ values of these fumaroles were $-2.8‰$ and $-3.1‰$. On the other hand, Sano and Williams (1996) reported a very low $\delta^{13}C$ (-6.94‰) for a high-temperature volcanic gas sample (965°C) from Pacaya, although limited additional information is associated with this value for evaluating the extent of air contamination and magmatic degassing. In terms of $^{3}He/^{4}He$ ratio, only five data points (1 fluid inclusion and 4 fumaroles) are available from previous studies and yielded values between 2.9 and 7.9 Ra (Goff et al., 2000; Poreda & Craig, 1989; Sano & Williams, 1996), indicating the influence of crustal contamination by radiogenic ^{4}He modifying the pristine signature. The volcano's SO_2 flux emissions have been repeatedly quantified in the past (Andres & Kasgnoc, 1998; Andres et al., 1993; Bluth et al., 2007; Dalton et al., 2010; GVN Bullettin, 2002; Rodríguez et al., 2004), but the fluxes of the two major magmatic gas components, H_2O and CO_2, have not yet been characterized.

Here, we report on the first magmatic gas (H_2O, CO_2, SO_2, H_2S, H_2) compositional data for Pacaya volcano. These results were obtained during a field campaign in January 2016, when a fully autonomous Multi-component Gas Analyser System (Multi-GAS) was deployed for 8 consecutive days on the rim of the Mackenney cone to measure the composition of the bulk plume released during continuous open-vent intra-crateric Strombolian activity. We combine these compositional data with simultaneous measurement of the volcanic SO_2 flux, obtained by a dual-UV Camera system (Tamburello et al., 2012), to assess the Total ($H_2O+CO_2+SO_2$) Volatile Flux (TVF) from Pacaya. The source (mantle versus slab) origin of the emitted magmatic volatiles is also explored by putting the inferred CO_2/SO_2 signature of Pacaya gas in the context of

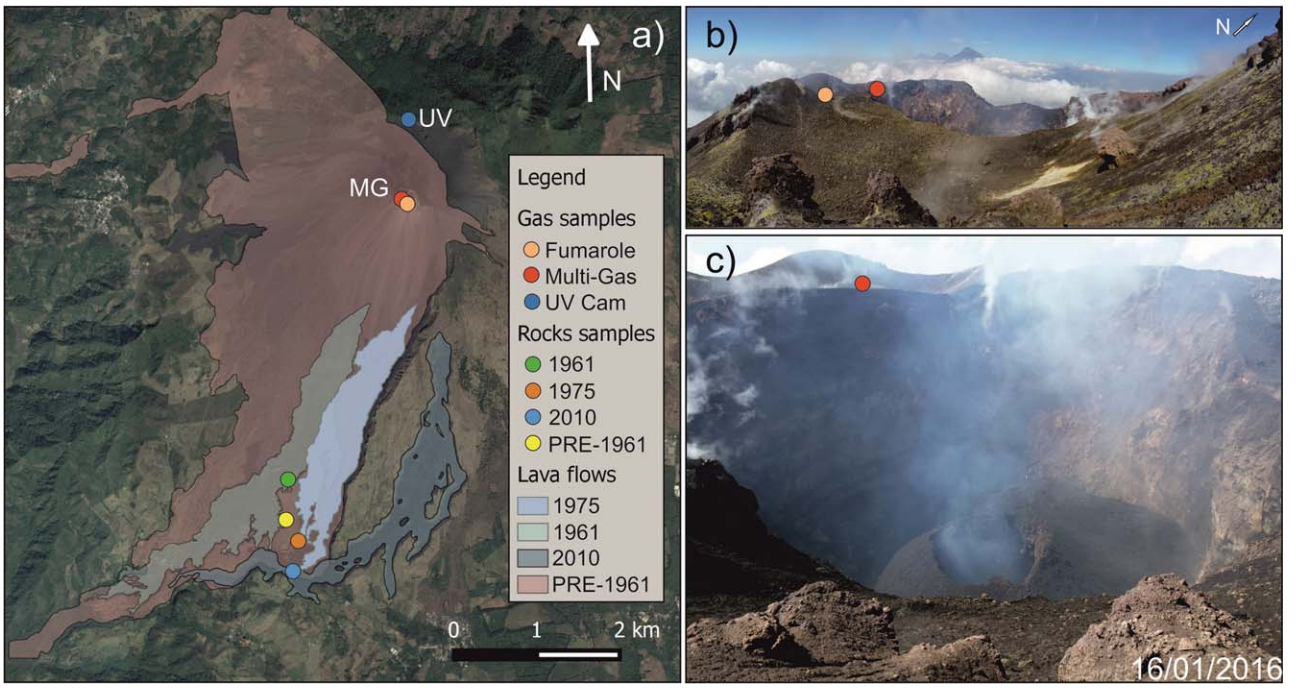

Figure 2. (a) Simplified geological map of Pacaya volcano, modified from Matías Gómez et al. (2012). The figures shows fumarole and rock sampling sites, the UV camera measurement site (UV Cam), and the Multi-GAS installation site (MG); (b) view of Pacaya crater taken from the south-eastern crater rim. Fuego volcano is visible in the background. Symbols are as in Figure a; (c) View of Mackenney crater, taken from south-eastern portion of the crater rim. The Multi-GAS installation site is shown by red circle.

regional (CAVA) gas versus trace element (in source magmas) relationships (Aiuppa et al., 2014, 2017), and by reporting on the first $^{3}He/^{4}He$ results for olivine-hosted fluid inclusions from a set of recent Pacaya lavas.

2. Geological, Volcanological, and Geochemical Background

2.1. CAVA and Guatemala

The Central American Volcanic arc is a 1,100 km-long volcanic front stretching along the continental margin associated with subduction of the Cocos plate beneath the Caribbean plate (Figure 1). The convergence rate between the Cocos and Caribbean plates gradually increases toward the southeast, from about 7 to 9 cm/yr (DeMets, 2001) (Figure 1). The age of the subducting Cocos lithosphere is approximately constant (about 26 Ma) along most part of the subduction zone, except along its south easternmost segment in central Costa Rica (17 to 25 Ma). The subducting lithosphere is divided into two segments by the Cocos Ridge, offshore of southern Costa Rica. The north-western segment is made of older and colder Cocos materials subducting at a relatively steep angle (65°) below El Salvador and Nicaragua, and at 55° beneath Guatemala (Syracuse & Abers, 2006). The Cocos Ridge is generated by separation of the Cocos and Nazca Plates and is consequently younger and warmer (Chan et al., 2002). According to Carr (1984) and Case et al. (1990), crustal thickness decreases from Guatemala (50-40 km) to Nicaragua (30 km), increases across Costa Rica and western Panama and then again thins in central Panama.

Variations in subduction parameters, including dip-angle, crustal thickness, extent of sediment underplating, faulting style and subduction erosion (Carr, 1984, Carr & Feigenson, 1990; Patino et al., 2000, Walker et al., 2001), control the degree of source melting and determine a variable sedimentary fluid influx from the subducting Cocos plate. These in turn determine large along-arc geochemical variations in Central American lavas (Carr & Feigenson, 1990; Leeman et al., 1994; Morris et al., 1990), with trace element proxies for slab fluids (such as Ba/La, U/Th, and Sr/Ce ratios) being highest in Nicaragua, and lowest in Costa Rica (Sadofsky et al., 2008). The same geochemical tracers indicate that melts beneath Guatemala are generated by mixing of a Costa Rica MORB-like melt component with Nicaragua-like slab fluid-rich melts (Sadofsky et al., 2008).

Volcanic gases do also exhibit significant along-arc variations. Fischer et al. (2002) showed that N isotopes and N_2/He ratios in geothermal fluids vary along the volcanic arc, and indicate lower slab fluid contributions in Costa Rica than Guatemala and Nicaragua. Similar variations have also been observed for He and C isotopes (Di Piazza et al., 2015; Leeuw et al., 2007; Robidoux et al., 2017; Shaw et al., 2003), pointing to higher influx and recycling of C-rich sediments beneath Nicaragua, and a minimal slab contribution in the volcanic output in Costa Rica, in spite of similar sedimentary inputs at the trench (Freundt et al., 2014). Barnes et al., (2009), studying chlorine isotope variations along the Central American volcanic front, similarly demonstrated mantle-like Cl signatures in the northernmost (Guatemala and El Salvador) and southernmost (Costa Rica) ends of the front, and sediment- and/or serpentinite-derived signature in Nicaragua. Consistent results were obtained by (Aiuppa et al., 2014) who explored the along-arc variations in volcanic gas CO_2/S ratios in the Costa Rica-Nicaragua segment of the arc.

Four different morphotectonic segments exist in Guatemala that result from the rotation of upper crustal blocks in northern Central America (Figure 1). Zone I is un-affected by Neogene extensional tectonics, while extensional regime in Zone II resulted in large volcanic rock productivity. Zones I and II are separated by the Atitlan caldera complex. The structural line between zone II and zone III is the Misto fault, which also corresponds to the western margin of the Guatemala graben (Figure 1), where the Amatitlan caldera complex is located. Zone III is a basin-and-range style structure and the principal movement is eastward, while Zone IV is characterized by arc-parallel pull apart-basins (Burkart & Self, 1985). In southern Guatemala, both E-W crustal extension (as evidenced by the existence of a series of N-S trending grabens (Burkart & Self, 1985); Figure 1) and right-lateral strike-slip movements (in the Jalpatagua Fault Zone, JFZ) are observed. Pacaya volcano lies at the intersection between the Guatemala graben and the JFZ (Cameron et al., 2003).

2.2. Pacaya Volcano

Pacaya volcano, one the most active volcanoes in Central America, is a large volcanic complex on the southern fault zone of the Amatitlan Caldera (Wunderman & Rose 1984), only 20 km south of the centre of Guatemala City, the Guatemala capital. The Pacaya volcanic complex comprises an ancestral andesitic stratovolcano, a series of rhyodacitic to andesitic lava domes, and the modern Pacaya basaltic composite volcano (2,552 m high) (Conway et al. 1992). Eggers (1971) subdivided the activity of Pacaya into three stages. Phase I was characterized by growth of a large, ancestral andesitic cone; this old volcano was largely eroded. The onset of phase II (about 0.16 Ma) was marked by an increase in the volcano's explosivity, with the eruption of voluminous pumice-bearing deposits, and the formation of andesitic-dacitic lava domes such Cerro Grande and Cerro Chiquito (these events are identified as phase III in (Bardinzteff & Deniel, 1992). Phase III started ~400 B.P. (divided in initial, historical, and modern sub-phases) and produced primarily basaltic lava flows through to the present day. These lavas are mostly porphyritic olivine-bearing basalts exhibiting no significant temporal chemical or petrographic variation (Bardinzteff & Deniel, 1992; Eggers, 1971). A series of collapse events affected ancestral Pacaya between 400 and 2,000 years B.P., forming a large collapse amphitheatre and a debris avalanche that traveled 25 km S-SW. Historical Pacaya encompasses the mid sixteenth century to 1861. Before this, Pacaya was possibly active in 1585, from ca. 1651 to 1678, and again in 1775 (Rose et al., 2013). After a repose period between 1860 and 1960, volcanic activity resumed in 1961 with modern Pacaya, which has since then shown nearly continuous strombolian activity and extrusion of lava from the Mackenney cone (Matías Gómez et al., 2012; Schaefer, 2012). The Mackenney cone, initially asymmetrical, began to grow in 1965 with the collapse of an amphitheatre that developed in 1961. There are not significant petrographic differences between initial, historic, and modern lavas, all showing olivine and plagioclase phenocrysts (up 45 wt. %) and microphenocrysts, and minor clino-pyroxene and magnetite microphenocrysts. Modern Pacaya lavas have progressively become slightly more mafic in composition (Bardinzteff & Deniel, 1992; Matías Gómez et al., 2012).

3. Materials and Methods

3.1. Multi-GAS

The composition of the Pacaya volcanic gas plume was investigated using a custom-made Multi-component gas analyzer system (Multi-GAS) (Aiuppa et al., 2005; Shinohara, 2005). Gas measurements were carried out during 14–22 January 2016, when a fully autonomous Multi-GAS was temporarily installed on Pacaya summit to measure the in-plume concentrations of CO_2, SO_2, H_2S, H_2 and H_2O. The Multi-GAS was installed

on the northwest rim of Mackenney cone (Lat, −14°22′55.48″N; Long 90°36′8.87″O), downwind the main direction of plume transport (Figure 2). The Multi-GAS was powered by an external (12 V, 40 Ah) battery, and acquired data at 0.1 Hz rate during 4 measurement cycles per day, each 30 minutes long (start time of the cycles, 00:00, 06:00 and 12:00, 18:00 GMT-time). SO_2, H_2S and H_2 concentrations were measured with specific electrochemical sensors (models TD2G-1A, TC4E-1A, TE1G-1A, respectively; all from City Technology). CO_2 concentrations were measured using an on-board spectrometer (Gascard EDI030102NG), while H_2O concentrations were derived from co-acquired temperature, pressure and humidity readings, as in previous work (Aiuppa et al., 2014, 2015). All data were acquired and stored in a Campbell scientific data logger (model CR6), and post-processed with the Ratiocalc software (Tamburello, 2015) to obtain ratios between volatile couples (Table 1). Ratiocalc automates the standard procedure (Aiuppa et al., 2005; Shinohara, 2005) of inferring volcanic gas ratios by taking the gradient of the best-fit regression lines in scatter plots of co-measured gas species concentrations. The error associated with each Multi-GAS derived ratio is $\leq \pm 20\%$ for CO_2/SO_2 and $\leq \pm 30\%$ for H_2O/SO_2 .

3.2. UV Camera

On 16 January, we used a dual-UV camera (same as in Tamburello et al., 2012) to acquire time-series of the volcanic SO_2 flux. Observations were carried out from an observational point situated on the northern volcano's flank (14°23′26.91″N, 90°36′5.91″O) at a distance of 940 m from the crater and 2,273 m elevation a.s.l. (see Figure 2) for 4 consecutive hours. The dual UV camera system used two co-aligned cameras (JAI CM 140 GR cameras, with 10 bit digitization and 1,392 × 1,040 pixels), with optical filters centred at either 310 nm (camera 1; affected by SO_2 absorption) or 330 nm (camera 2; not affected by SO_2 absorption). Absorbance *A* for each camera pixel was calculated as (Kantzas et al., 2010; Tamburello et al., 2012):

$$A = -\log_{10}[(IP_{310}/IB_{310})/(IP_{330}/IB_{330})] \quad (1)$$

where IP and IB are, respectively, dark image-subtracted plume and background sky images taken with the two co-exposed cameras. Image sequences were post-processed using the Vulcamera software (Tamburello et al., 2011) to derive time-series of integrated SO_2 column amounts (ICAs) along a cross section of the plume. These were converted into SO_2 fluxes multiplying by a time series of plume transport speed, with the average of 8.2 ± 4 m/s, derived by an optical flow algorithm integrated in Vulcamera (see D'Aleo et al., 2016, for details).

3.3. Direct Sampling

During the field campaign, we collected gas samples from two low-temperature fumaroles (80°C), located on the northwest rim of the Mackenney cone. These fumaroles were aligned along a 15–20 m radial fracture trending away from the crater. For each of the two fumaroles, we sampled two glass flasks. Due to the ongoing Strombolian activity, access to the eastern part of the inner crater, where higher temperature fumaroles are possibly present, was not possible due to safety reasons. During sampling, a stainless steel tube was inserted into the fumarolic vent until thermal equilibration with the fumarole gases. Then, a 3-way valve was connected to the tube, a 100 ml syringe and a glass flask in order to collect the gases. The collected gas samples were analyzed for their chemical composition and $\delta^{13}C$ of CO_2 at INGV (Table 2). The concentrations of He, H_2, O_2, N_2, CO, CH_4, and CO_2 were determined using a Perkin Elmer Clarus 500 gas chromatograph equipped with a 3.5-m Carboxen 1000 column and 2 detectors (a thermal conductivity and a flame ionization detector, respectively), with analytical errors of $< 3\%$. The C isotope composition of CO_2 (expressed as $\delta^{13}C$ ‰ versus V-PDB) was determined using a Thermo (Finnigan) Delta Plus XP CF-IRMS, connected to a Trace GC gas chromatograph and a Thermo (Finnigan) GC/C III interface. The gas chromatograph, equipped with a Poraplot-Q column (length 30 m, i.d. 0.32 mm), kept at a constant temperature of 50°C, uses He as the carrier gas. The analytical uncertainty was ± 0.1‰. Due to the high extent of air contamination, samples were not analyzed for noble gases.

3.4. Chemistry of Rocks and Olivine Crystals

In January 2016, fresh rock samples were collected on the southern flank of Pacaya volcano from outcrops of the following eruptions: Pre-1961 (Cerro Chino cinder cone and Pacaya composite cone with undivided lava flow, (Eggers, 1971); hereafter referred as pre-1961), 1961, 1975, and 2010. All samples are basaltic lava flows, according to modern Pacaya behavior. Outcrops were selected from volcanics of the recent eruptive activity that are richest in olivines (based on previous results in Bardinzteff & Deniel, 1992; Matías et al.,

Table 1
CO_2/SO_2 and H_2O/SO_2 Ratios in the Pacaya Plume Derived From Multi-GAS Measurements

Date	Start	End	SO_2 max	CO_2/SO_2	Error on CO_2/SO_2	H_2O/SO_2	Error on H_2O/SO_2
14/01/2016	00:13	00:15	8.2	2.6	0.5	22.0	6.6
14/01/2016	00:15	00:18	8.2	2.5	0.5	5.5	1.6
14/01/2016	18:12	18:21	6.1	10.3	0.8	157	47
14/01/2016	18:21	18:24	20	4.2	0.4	37.7	11.3
14/01/2016	18:25	18:29	20	4.3	0.4	70.8	21.2
15/01/2016	18:05	18:07	15	3.3	0.3	39.1	11.7
15/01/2016	18:08	18:10	15	3.3	0.3	35.9	10.8
15/01/2016	18:10	18:12	13	3.9	0.4	40.2	12.0
15/01/2016	18:12	18:16	13	3.8	0.4	83.0	24.9
15/01/2016	18:16	18:19	14	3.6	0.3	10.2	3.1
15/01/2016	18:20	18:23	14	3.5	0.3	44.8	13.4
16/01/2016	00:24	00:27	20	1.6	0.2	13.1	3.9
16/01/2016	00:27	00:29	20	1.5	0.2	11.7	3.5
16/01/2016	06:02	06:12	23	0.9	0.1	5.2	1.6
16/01/2016	06:06	06:08	11	2.1	0.2	8.8	2.7
16/01/2016	06:09	06:11	22	0.8	0.1	12.3	3.7
16/01/2016	06:14	06:18	22	1.5	0.2	20.6	6.2
16/01/2016	06:20	06:23	44	0.7	0.1	39.2	11.8
16/01/2016	06:24	06:26	34	0.9	0.1	8.9	2.7
16/01/2016	06:27	06:30	34	0.9	0.1	32.4	9.7
16/01/2016	18:00	18:05	4.3	9.8	1.0	329	98
17/01/2016	06:02	06:04	4.5	5.1	0.9	134	40
17/01/2016	06:05	06:08	4.5	5.0	0.9	39.6	11.9
18/01/2016	06:09	06:13	62	0.7	0.1	6.1	1.8
18/01/2016	06:14	06:20	40	0.7	0.1	1.7	0.5
18/01/2016	06:21	06:23	40	0.8	0.1	10.5	3.1
18/01/2016	06:24	06:27	40	0.7	0.1	6.5	1.9
18/01/2016	12:12	12:16	43	1.2	0.1	7.7	2.3
18/01/2016	18:00	18:04	22	2.9	0.2	116	34.9
18/01/2016	18:05	18:10	22	3.3	0.1	74.2	22.3
18/01/2016	18:11	18:14	22	2.9	0.2	109	32.7
18/01/2016	18:15	18:17	22	3.3	0.1	32.5	9.7
18/01/2016	18:18	18:20	5.1	8.5	1.0		
18/01/2016	18:22	18:26	5.1	8.2	1.0	194	58.3
19/01/2016	06:07	06:09	21	1.6	0.2	9.2	2.8
19/01/2016	06:09	06:12	21	1.5	0.2	1.6	0.5
19/01/2016	06:24	06:26	27	1.0	0.1	28.9	8.7
19/01/2016	06:27	06:30	27	1.1	0.1	1.5	0.4
20/01/2016	18:16	18:22	17	2.4	0.7	33.8	10.2
20/01/2016	18:22	18:24	47	1.3	0.4	4.5	1.3
20/01/2016	18:25	18:28	47	1.2	0.4	10.7	3.2
21/01/2016	00:01	00:20	66	0.9	0.3	4.2	1.3
21/01/2016	00:22	00:29	66	0.9	0.3	8.9	2.7
21/01/2016	18:08	18:12	6.4	6.0	1.8	131	39.4
21/01/2016	18:12	18:14	6.0	6.6	2.0	-	-
21/01/2016	18:16	18:19	6.0	6.7	2.0	60.3	18.1
21/01/2016	18:20	18:23	6.5	5.4	1.6	78.2	23.5
21/01/2016	18:24	18:26	6.5	5.4	1.6	89.8	26.9
21/01/2016	18:27	18:28	29	0.9	0.3	12.7	3.8
21/01/2016	18:28	18:29	29	0.9	0.3	11.8	3.5
22/01/2016	00:03	00:05	23	2.0	0.6	24.5	7.4
22/01/2016	00:06	00:10	23	1.9	0.6	14.8	4.4
22/01/2016	00:11	00:14	49	1.0	0.3	35.0	10.5
22/01/2016	00:15	00:17	49	1.0	0.3	4.5	1.4
22/01/2016	00:17	00:20	21	2.4	0.7	39.7	11.9
22/01/2016	00:21	00:24	21	2.5	0.7	11.1	3.3
22/01/2016	00:28	00:29	42	1.3	0.4	10.1	3.0
22/01/2016	12:00	12:28	82	1	0.3	22.8	6.8

Table 1. (continued)

Date	Start	End	SO_2 max	CO_2/SO_2	Error on CO_2/SO_2	H_2O/SO_2	Error on H_2O/SO_2
22/01/2016	18:00	18:25	114	0.8	0.2	9.2	2.8
22/01/2016	00:27	00:30	42	1.3	0.4	12.7	3.8

Note. Each value corresponds to the average ratio obtained within a short (a few minutes long) temporal window, calculated from the slope of the best-fit regression line between co-acquired CO_2 and SO_2 and H_2O and SO_2 concentrations, respectively (see examples of two temporal intervals in Figure 3). Duration (start and end time) of each of these temporal windows is indicated in the Table. For each ratio, the quoted error represents the confidence radius of the slope calculated with a level of certainty of 99.99%, and corresponds to the probability that the best fit falls between lower and upper bounds. This depends on the number of samples and the quality of the best-fit, and therefore changes from ratio to ratio. SO_2 max is the peak SO_2 concentration (in ppm) in the plume measured within each considered temporal window.

2012; Rose et al., 2013; Wardman et al., 2012). Olivine phenocrysts are the most suitable for studying He, Ne, and Ar in fluid inclusions (FI), because they effectively retain the small helium atoms within the crystal's structure, thus avoiding (or reducing) any diffusive effect. In addition, olivines are among the first mineral phases crystallizing from a basaltic melt. The collected rocks were initially characterized for their whole-rock chemistry and mineral chemistry of olivine host crystals. Major and trace elements in whole rocks (supporting information Tables S1 and S2) were measured at the Activation Laboratories (Canada) using inductively coupled plasma–mass spectrometry (ICP-MS), in which rock samples digested under acidic attack were analyzed by a Perkin Elmer Sciex ELAN 6000, 6100, or 9000 ICP-MS device. Duplicate measurements indicate reproducibility was generally better than 3% for major-element analyses, 5% for highly incompatible elements (i.e., Rb, Ba, U, and Th), and 7% for rare-earth elements. Accuracy was quantified by comparing measured and certified values for standard references (NIST694, DNC-1, GBW, W-2a, SY-4, and BIR-1a).

Olivine phenocrysts were then handpicked, prepared on Crystal-Bond™ resin, and polished on one side in order to have a flat surface. Major elements (supporting information Table S3) were determined using a JXA-8200 combined WD/ED (energy-dispersive) electron microprobe (EMPA) at the High Pressure and High Temperature Laboratory of INGV, Sezione di Roma 1. The analytical conditions were a beam current of 7.5 nA, accelerating voltage of 15 kV, and beam size of 5 μm with counting times of 10 and 5 s for peaks and the background, respectively.

3.5. Noble Gas Isotopes in Fluid Inclusions

Olivine crystals were separated from the four rock samples previously fragmented and sieved in the fractions of 0.5 and 1 mm, with the aim of studying fluid inclusions trapped therein. Fluid inclusions are small (from tens to few microns in diameter) bubbles of fluid (generally gas) trapped within minerals during olivine growth at magmatic conditions. This means gases trapped in fluid inclusions represent an early stage of degassing, especially in olivine crystals that crystallize early from basaltic melts. The procedure of sample preparation and analysis is described in Di Piazza et al. (2015) and Robidoux et al. (2017). In samples from 1961, 1975, and 2010 eruptions, olivine crystals were separated in the two fractions (0.5 and 1 mm), while from pre-1961 only in the 0.5 mm fraction. Aliquots of 0.2 to 0.7 g were analyzed by single-step crushing in replicate measurements for elemental and isotope composition of helium, neon, and argon in fluid

Table 2
Chemistry (in ppm and % vol.) and Carbon Isotope Composition (V-PDB) of Gases Collected From the Two Fumaroles at Pacaya Volcano

Sample	Date	T (°C)	He (ppm)	H_2 (ppm)	O_2 (%)	N2 (%)	CH_4 (ppm)	CO (ppm)	CO_2 (%)	δ^{13} C CO_2 (‰)
PA-1	22/01/2016	80	6	64	19.33	76.78	1.3	58	2.34	−3.9
PA-1 bis	22/01/2016	80	-	90	19.19	76.78	0.5	83	2.83	−4
PA-2	22/01/2016	80	-	71	20.05	77.83	0.8	1.5	0.93	−3.7
PA-2 bis	22/01/2016	80	-	629	20.11	77.57	0.7	167	0.96	−3.8

Note. Analytical uncertainty is $< 3\%$ for chemical composition and $\pm 0.1‰$ for δ^{13}C.

Table 3
Noble Gas Concentration and Isotope Composition in Olivine-Hosted Fluid Inclusions

Sample	Mineral	Weight of loaded minerals (g)	Crystal size fraction (mm)	[^{4}He] (mol/g)	[^{20}Ne] (mol/g)	[^{40}Ar] (mol/g)	[^{36}Ar] (mol/g)	^{40}Ar/^{36}Ar	Error on (^{40}Ar/^{36}Ar) (%)	^{38}Ar/^{36}Ar	Error on (^{38}Ar/^{36}Ar) (%)	R/Ra	^{4}He/^{20}Ne	Rc/Ra	Error +/-
2010	Ol	0.23130	1	1.4E-13	5.3E-15	2.2E-13	7.3E-16	298.4	0.9	0.218	0.2	8.77	25.8	8.87	0.2
1961	Ol	0.19088	1	2.2E-13	4.8E-15	2.7E-12	9.0E-15	302.5	0.1	0.188	0.2	8.55	45.7	8.61	0.2
2010	Ol	0.48897	1	1.9E-13	7.4E-15	6.7E-13	2.0E-15	328.5	0.3	0.191	0.2	8.76	25.5	8.87	0.1
2010	Ol	0.74272	0.5	1.3E-13	1.2E-15	6.9E-13	2.2E-15	313.6	0.1	0.189	0.2	8.46	113.5	8.48	0.1
1975	Ol	0.41451	0.5	2.0E-13	3.2E-15	1.5E-12	5.0E-15	313.4	0.2	0.187	0.2	8.52	64.8	8.56	0.1
1961	Ol	0.45078	0.5	1.0E-13	2.2E-15	1.1E-12	3.6E-15	303.9	0.1	0.187	0.2	8.33	46.8	8.38	0.2
1961	Ol	0.47792	0.5	1.1E-13	3.6E-15	1.6E-12	5.4E-15	300.1	0.1	0.186	0.2	8.58	31.0	8.67	0.2
PRE- 1961	Ol	0.45588	0.5	1.1E-13	3.1E-15	5.2E-13	1.7E-15	309.3	0.2	0.193	0.2	8.36	37.2	8.43	0.2
2010	Ol	0.67055	0.5	1.2E-13	2.7E-15	1.2E-12	3.9E-15	303.3	0.1	0.187	0.2	8.98	45.5	9.04	0.1
1975	Ol	0.41887	0.5	7.8E-14	3.7E-15	7.0E-13	2.3E-15	301.9	0.2	0.187	0.2	8.46	21.1	8.58	0.2
1975	Ol	0.41702	1	2.7E-13	8.2E-15	1.5E-12	3.2E-15			0.187	0.2	8.77	32.9	8.82	0.2
1975	Ol	0.53080	1	1.5E-13	1.5E-15	9.8E-13	3.2E-15	308.7	0.1	0.189	0.2	8.58	102.0	8.61	0.2
PRE-1961	Ol	0.50041	0.5	9.4E-14	3.1E-15	5.3E-13	1.7E-15	305.3	0.2	0.191	0.2	8.44	30.7	8.52	0.2

inclusions hosted in olivine crystals (Table 3). These analyses were performed at the noble gas isotope laboratory of INGV, Sezione di Palermo, following internal protocol (e.g., Di Piazza et al., 2015; Rizzo et al., 2015; Robidoux et al., 2017). Helium isotopes (^{3}He and ^{4}He) and ^{20}Ne were measured separately by two different split-flight-tube mass spectrometers (Helix SFT-Thermo). The ^{3}He/^{4}He ratio is expressed normalized to Ra (where Ra is the ^{3}He/^{4}He of air; i.e., 1.39×10^{-6}). The analytical uncertainty of He isotope ratio measurements was $\leq$2.5%. The ^{3}He/^{4}He ratios were corrected for atmospheric contamination based on the measured ^{4}He/^{20}Ne ratio (e.g., Sano & Wakita, 1985) and are expressed as Rc/Ra values. Argon isotopes (^{36}Ar, ^{38}Ar, and ^{40}Ar) were analyzed by a multicollector mass spectrometer (GVI Argus) at an analytical uncertainty of $\leq$0.9% (Table 3). The uncertainty in the measured amounts of He, Ne, and Ar elements was $<$5%. Typical blanks for He, Ne, and Ar were $<10^{-14}$, $<10^{-16}$ and $<10^{-14}$ mol, respectively, and were at least 1–2 orders of magnitude lower than values measured in the samples.

4. Results

4.1. Plume Composition and SO_2 Fluxes

During our observations on 14–22 January 2016, mild Strombolian activity persisted at a small pyroclastic cone inside the MacKenney crater (Figure 2). Larger explosions, interspersed within continuous degassing and spattering activity, produced $<$100m high columns that deposited scoriae and bombs, mostly inside the inner crater. No major change in activity was observed during our reporting period, except for a small collapse event of the north-western sector of the crater on January 20 that produced a gray ash-rich column (INSIVUMEH, monthly report January 2016). Direct observations indicated that intra-crateric Strombolian activity was somewhat more intense on 20–21 January, when some bombs reached the outer crater rim and damaged the outer case of the Multi-GAS.

The volcanic plume was dispersed toward north/north-west (e.g., toward the Multi-GAS measurement site) throughout most part of the Multi-GAS measurement interval, allowing regular plume detection (Figure 2). The maximum gas concentrations we measured in the Pacaya plume were 120 ppm (SO_2), 550 ppm (CO_2), 1.5 ppm (H_2), and 3,000 ppm (H_2O) (this latter is the excess H_2O content above an atmospheric background of 15,000–19,000 ppm). H_2S concentrations were typically below the sensor's 13% cross sensitivity to SO_2, and we therefore infer the Pacaya plume was typically H_2S-poor (at $<$1 ppm level). Occasionally, due to unfavorable plume transport directions, the Multi-GAS sensed a very dilute plume and/or the gas emitted from low temperature fumaroles in the inner crater's wall, close to the measurement site.

Figure 3 is a scatter plot of pairs of co-acquired CO_2 and SO_2 concentration data. The plot demonstrates that plume CO_2/SO_2 (molar) ratios fluctuated from $<$1 to $>$10 during the study period. This spread of CO_2/SO_2

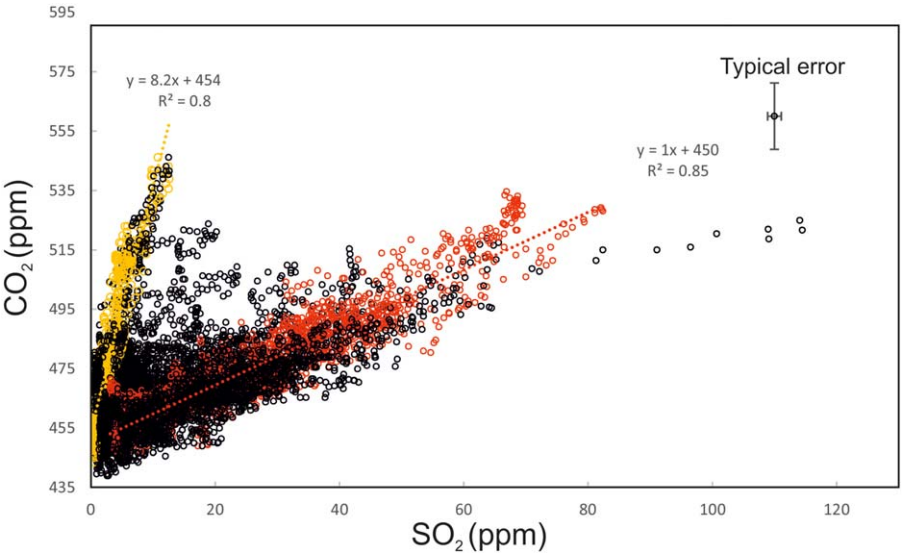

Figure 3. Scatter plot of pairs of co-acquired CO_2 and SO_2 concentrations in the Pacaya plume. Open black circles identify all couples of co-acquired CO_2 and SO_2 obtained during January 14–22. We show results for all temporal windows in which CO_2 and SO_2 were correlated at significant levels ($R^2 > 0.8$) (implying plume fumigation at the Multi-GAS measurement site), and that concurred to calculation of the CO_2/SO_2 ratios listed in Table 1. The spread of compositions imply a large variability of CO_2/SO_2 ratios during January 14–22 (see Table 1). CO_2/SO_2 ratios were more constant on shorter timescales, e.g., over temporal timescales of minutes. We thus selected using the software Ratiocalc (Tamburello, 2015) a sequence of short (a few minutes long) temporal windows, in each of which the mean CO_2/SO_2 ratio was calculated from the slope of the best-fit regression line in CO_2 versus SO_2 concentration plots. Results for two representative measurement intervals are shown in the Figure. Yellow circles: CO_2 versus SO_2 sub-population for the 6:22-6:26 pm (GMT time) acquisition on January 18. The best-fit regression line has a slope of 8.2 ($R^2 = 0.8$). Red circles: CO_2 versus SO_2 sub-population for the 12:00–12:28 (GMT time) acquisition on January 22. The best-fit regression line has a slope of 1 ($R^2 = 0.85$). Note the intercepts of both regression lines ($CO_2 \sim 450$ ppm) are well-above CO_2 levels in background air (~ 400 ppm), suggesting diffuse CO_2 loss from soils and warm grounds in the crater area. The typical errors in CO_2 and SO_2 concentrations are shown by the error bar.

ratios is evident from comparison of CO_2 versus SO_2 sub-populations taken in two distinct measurement intervals (red: 22 January; yellow; 18 January), in which the slopes of the best-fit regression lines are 1 and 8.2, respectively. In view of this temporal variability, we calculated (using Ratiocalc) the "mean" CO_2/SO_2 ratio in individual, few minutes-long, temporal intervals, during which the plume was compositionally more constant (e.g., the obtained correlation coefficients between CO_2 and SO_2 concentrations were high: R^2 from 0.60 to 0.91). The obtained CO_2/SO_2 ratios ranged from 0.6 to 10.5 (Table 1), and their average (arithmetic mean) was 3.0 ± 2.7 (1 standard deviation, SD). In Figure 4a, the obtained CO_2/SO_2 ratios are plotted against the peak SO_2 concentration measured in the corresponding temporal window (see Table 1). This peak SO_2 concentration is here taken as a "plume marker," e.g., as a proxy for the density of the plume at the measurement site. We find that CO_2/SO_2 ratios are widely scattered and typically higher (mostly between 2 and 10.5) at low SO_2 (< 20 ppm) concentrations (dilute plume conditions), while they converge to low values (between 0.5 and 1.5) at higher peak SO_2 concentrations (dense plume conditions). A similar behavior is also observed for H_2O/SO_2 (Figure 4b), in which stable and low ratios (range 2–20; average ~ 11) are obtained in dense plume conditions (peak SO_2 concentrations > 20 ppm). We also derived plume H_2/SO_2 ratios of 0.01 to 0.3, with a cluster at 0.04 ± 0.01 in the subset of high SO_2 concentration data. Although H_2S/SO_2 ratios were not detected, we inferred a maximum ratio of 0.05 based on H_2S being below detection in all acquisitions. SO_2 was therefore the only substantial S component in the plume (i.e., $SO_2 \approx$ Total Sulfur, S_t).

Figure 5a is a pseudo-color image of SO_2 column densities (in ppm·m) in the Pacaya plume, obtained from processing of couples of co-acquired images taken by our UV camera system in the morning of January 16, 2016. During the measurements, the plume was nearly transparent and vertically lofting above the crater (Figure 5b). Sequences of images such as that shown in Figure 5a were obtained every 3 seconds. These were processed to obtain time-series of SO_2 ICA, using a cross section orthogonal to the plume transport

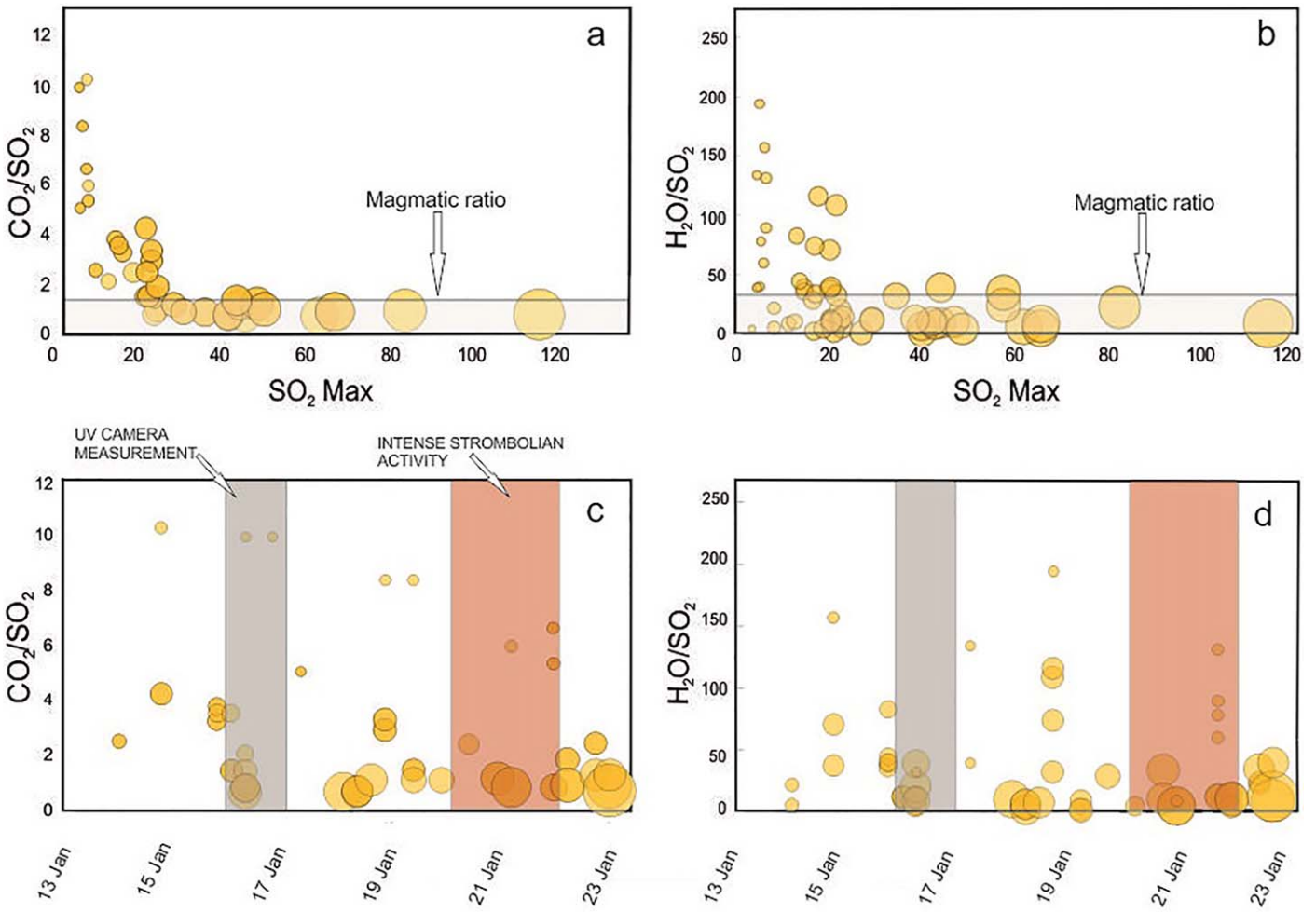

Figure 4. The CO_2/SO_2 and H_2O/SO_2 ratios obtained in individual acquisition windows (see Table 1). In each panel, size of bubbles is proportional to the peak (maximum) SO_2 concentration detected during each temporal window (listed in Table 1). (a and b), ratios are plotted as a function of peak SO_2 concentrations. In both plots, CO_2/SO_2 and H_2O/SO_2 ratios are scattered at low SO_2 concentrations and converge to a narrow "magmatic" range (of 0.5-1.5 and 2–20, respectively) at high (> 20 ppm) SO_2 concentrations. (c and d) Temporal plots of CO_2/SO_2 and H_2O/SO_2 ratios, respectively. Grey and red shaded areas mark the UV camera measurement interval and a phase of especially intense strombolian activity, respectively.

direction (see Figure 5a). From these, and by using a plume transport speed of 8.2 ± 4 m/s, the SO_2 flux time-series of Figure 5c was obtained. The derived SO_2 fluxes varied largely, from ~100 to 4,210 tons/d, consistent with visual observations (from the crater rim) of fluctuations in explosive and degassing activity at the pyroclastic cone inside the MacKenney crater. We caution that part of the large SO_2 flux temporal variability was caused by passage of clouds between ~16:50 and ~17:20 GMT, which partially obscured view of the crater area and resulted into reduced SO_2 fluxes (Figure 5c). Excluding this subset of values, we obtain an averaged SO_2 flux of 885 ± 550 tons/d.

4.2. Chemical and Carbon Isotope Composition of Fumarole Gases

The chemistry of gases collected from the two low-temperature fumaroles displayed a strong air contamination, as demonstrated by the dominant O_2 and N_2 composition (19.3%, 76. 8% respectively; Table 2). CO_2 concentrations were between 0.9 and 2.8%. The $\delta^{13}C$ of CO_2 varied in a narrow range, from −3.7‰ to −4.0‰. Based on theoretical values in air of CO_2 and $\delta^{13}C$ (CO_2≈400 ppm and $\delta^{13}C$=-8‰), we calculated a fraction of contamination in our samples. Then, we used an isotope balance to quantify the effect of air mixing and recalculate the air-corrected magmatic gases $\delta^{13}C$. This procedure yields $\delta^{13}C$ of CO_2 between −3.5 and −3.9‰ (Table 2).

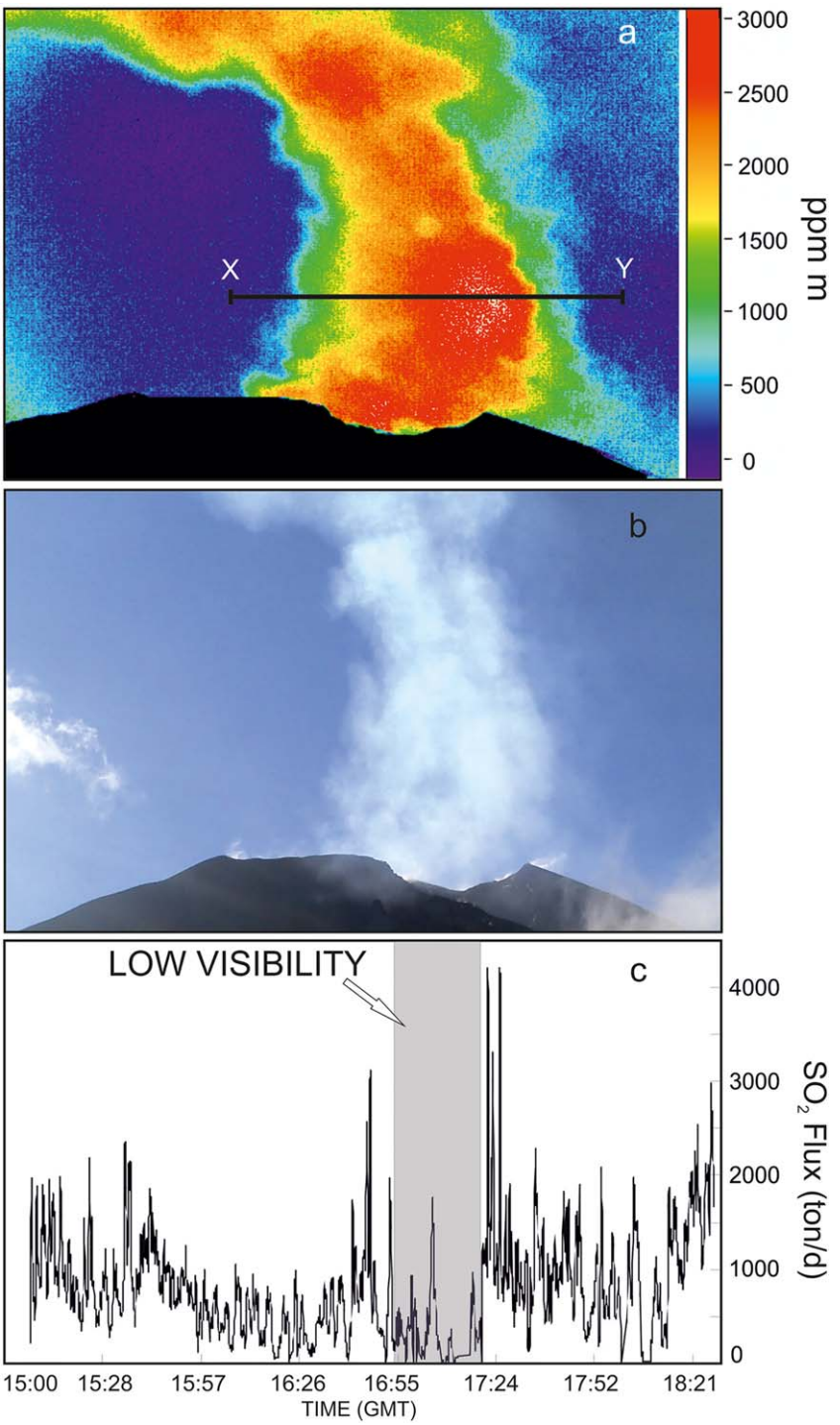

Figure 5. (a) Pseudo-color image showing SO_2 slant column amounts (expressed in ppm·m) in the Pacaya plume, as derived from UV camera measurements. The horizontal X-Y section indentifies location of the orthogonal cross section used to derive SO_2 ICAs (Integrated Column Amounts). (b) Visible image of the Pacaya plume, taken from the same UV Camera measurement site (see Figure 1a). (c) SO_2 flux time-series obtained for the 4-hours long UV Camera acquisition period on 16 January 2016. The grey shaded area identifies a period of reduced visibility due to cloud passage.

4.3. Chemistry of Whole Rocks and Olivine Crystals

The whole-rock composition of the studied samples is basaltic, with SiO_2 contents between 50.2 and 50.7 wt. % and total alkalis ($Na_2O + K_2O$) between 3.8 and 4.1 wt%. The MgO content is generally comprised

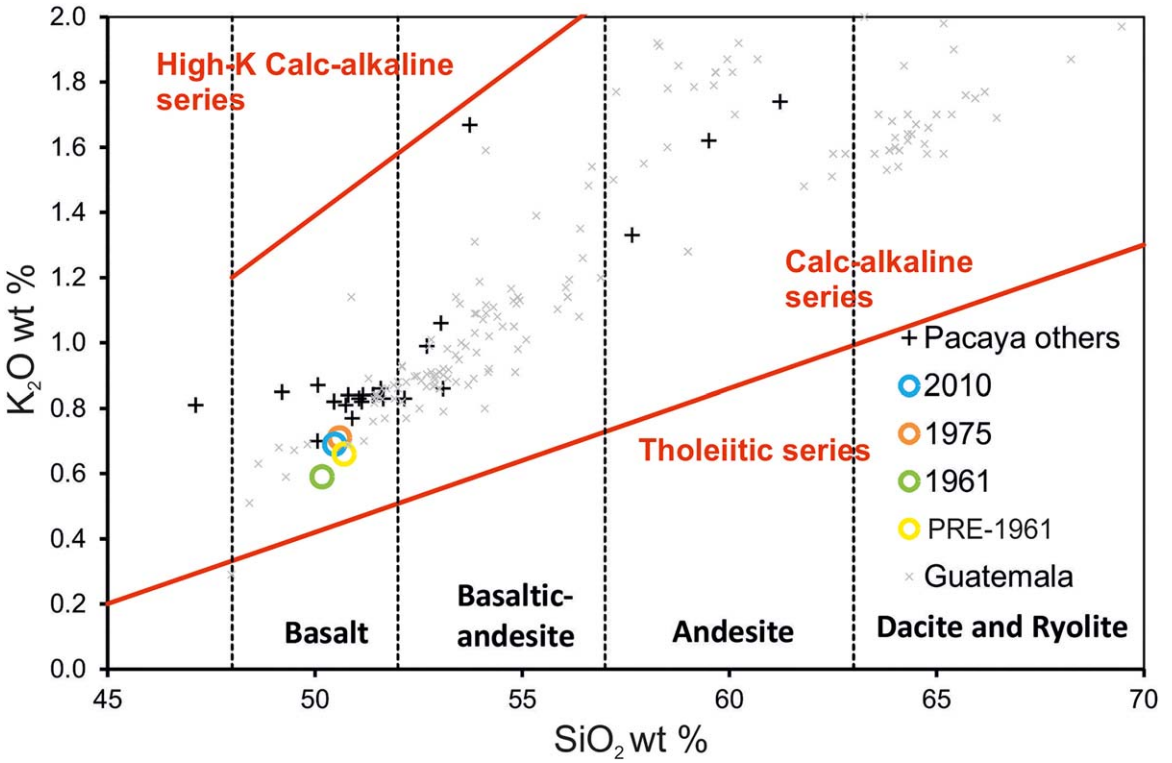

Figure 6. K_2O versus SiO_2 plot for whole-rock Pacaya samples, modified from Peccerillo and Taylor (1976). Our samples (see legend) are compared with literature information on rocks from Pacaya and Guatemala. Black crosses referred as "Pacaya others" in the legend correspond to published results (data from Bardintzeff & Daniel, 1992; Cameron et al., 2003; Carr & Feigenson, 1990; Carr et al., 1984; Chan et al., 2002; Feigenson & Carr, 1986; Leeman et al., 1994; Morris et al., 1990; Noll et al., 1996; Patino et al., 2000; Walker et al., 2007, 2009)). The grey crosses referred as "Guatemala" in the legend correspond to published whole-rock information on Guatemalan volcanoes (data extracted from the earthchem portal; http://www.earthchem.org/portal).

between 2.9 and 4.0 wt. %, while total Fe varies between 7.9 and 9.5 wt%. These results agree well with published data on the same eruptions (Bardinzteff & Deniel, 1992; Matías et al., 2012; Rose et al., 2013; Wardman et al., 2012), and confirm the basaltic composition of most of the products erupted from the volcano since historic time. In the K_2O versus SiO_2 classification diagram (Figure 6; after Peccerillo & Taylor, 1976), Pacaya volcanics spread over the typical compositional field of the calc-alkaline magmatic series. Rock samples investigated in this work are among the most mafic ever erupted at Pacaya and in Guatemala (Figure 6). Pacaya lavas also have relatively low fluid–mobile to less-fluid–mobile trace element ratios (Ba/La = 46.23 ± 2.2; U/Th = 0.42 ± 0.04; Ba/Th = 350 ± 18) (see also Heydolph et al., 2012), and plot therefore at the lower limit of the CAVA compositional range (Sadofsky et al., 2008). These low ratios suggest limited contribution from sediments in the subducted slab (Sadofsky et al., 2008).

Olivine phenocrysts (~10 vol.%), separated for the noble gases investigation in fluid inclusions, have euhedral to sub-hedral habitus and display a broad range of compositions at cores (Fo_{65}–Fo_{90}), with an unimodal distribution (mode at Fo_{65}–Fo_{73}) that suggests the lack of clear mixing processes.

4.4. Noble Gases in Fluid Inclusions

The ^4He content in olivine crystals ranges between 7.8×10^{-14} and 2.7×10^{-13} mol/g (Figure 7), ^{20}Ne varies from 1.2×10^{-15} to 8.2×10^{-15} mol/g, while ^{40}Ar between 2.2×10^{-13} and 2.7×10^{-12} mol/g. No systematic difference in concentrations is observed among the samples. All the data fall in the concentration range of the 1975 samples (Figure 7). The $^4He/^{20}Ne$ ratio is an indicator of atmospheric contamination and ranges between 21 and 113, which is at least 66 times higher than the typical atmospheric ratio ($^4He/^{20}Ne = 0.318$). In Figure 8, we plot our data in order to evaluate the extent of air contamination. To do this we assume a binary mixing between an atmospheric end-member, having $^4He/^{20}Ne = 0.318$ and R/Ra = 1, and two magmatic end-members, having $^4He/^{20}Ne = 1{,}000$ and Rc/Ra of either 8.3 or 9.0. These two mixing curves practically cover the entire dataset of fluid inclusions, indicating that the magmatic

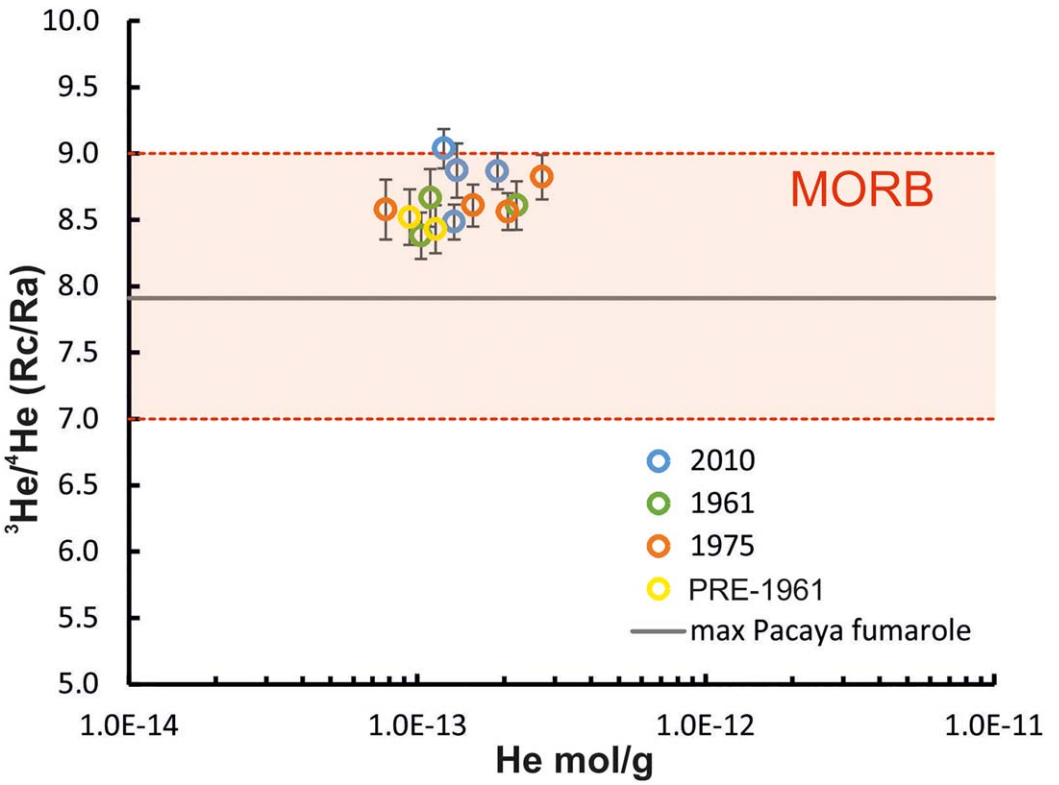

Figure 7. Air-corrected $^{3}He/^{4}He$ ratios (expressed as Rc/Ra) versus He content (mol/g) in FIs hosted in olivine minerals. Our data are compared with the MORB range (7–9 Ra), taken from Graham (2002), see light orange area. The highest $^{3}He/^{4}He$ ratio measured in the Pacaya summit fumaroles in the 1990s (Goff et al., 2000) is shown by the dashed grey line.

end-member varies in this range of $^{3}He/^{4}He$ ratio (8.3–9.0 Ra, Figure 8). The $^{40}Ar/^{36}Ar$ varies from 298 to 328, which is slightly higher than atmospheric ($^{40}Ar/^{36}Ar = 295.5$). Both $^{4}He/^{20}Ne$ and $^{40}Ar/^{36}Ar$ ratios are lower than those typical of fluids from the upper mantle ($^{4}He/^{20}Ne > 1{,}000$ and $^{40}Ar/^{36}Ar > 40{,}000$; Ozima & Podosek, 1983), but fall within the range of subduction-related volcanism worldwide and in CAVA (Di Piazza et al., 2015; Fischer et al., 2005; Hilton et al., 2002; Rizzo et al., 2015; Robidoux et al., 2017). This indicates that gases released from FIs contain an atmospheric-derived component, perhaps related to the recycling of noble gases in the subducting slab.

We selected the subset of samples having $^{40}Ar/^{36}Ar > 300$ and calculated the air-corrected ^{40}Ar content assuming that all the measured ^{36}Ar is atmospheric in origin:

$$^{40}Ar* = {}^{40}Ar_m - (({}^{40}Ar/{}^{36}Ar)_{air} \times {}^{36}Ar_m) \quad (2)$$

In relation (2), $^{40}Ar^*$ is the air-corrected ^{40}Ar, and the "m" subscript indicates "measured." The $^{40}Ar^*$ was not calculated for the 2010 eruption samples ($^{40}Ar/^{36}Ar < 300$) and for one 1975 sample (for which the $^{40}Ar/^{36}Ar$ was not determined). The recalculated $^{4}He/^{40}Ar^*$ varies between 2.3 and 5.5, which is within the typical production ratio of the mantle ($^{4}He/^{40}Ar^* = 1–5$; Marty, 2012; Ozima & Podosek, 1983). Considering that He is around 10 times more soluble than Ar in silicate melts, magmatic degassing would lead to an increase of $^{4}He/^{40}Ar^*$ especially in the late stages of degassing (e.g., Iacono-Marziano et al., 2010). Thus, the small variability of this ratio in our fluid inclusions suggests that olivine crystals were entrapped in a small pressure range.

The $^{3}He/^{4}He$ ratios corrected for atmospheric contamination vary from 8.4 to 9.0 Ra (Figure 7). These ratios are within the MORB-like range ($R/Ra = 8.0 \pm 1$; Graham, 2002), and are sensibly higher than the four data previously available results for Pacaya (Figure 7). The reported $^{3}He/^{4}He$ ratios in the three volcanic gases collected in the 1990s (Sano & Williams, 1996; Goff et al., 2000) vary between 2.9 and 7.9 Ra, and a single R/Ra of 6.8 ± 1.5 Ra was obtained for the only available olivine phenocrysts measurement (Poreda & Craig,

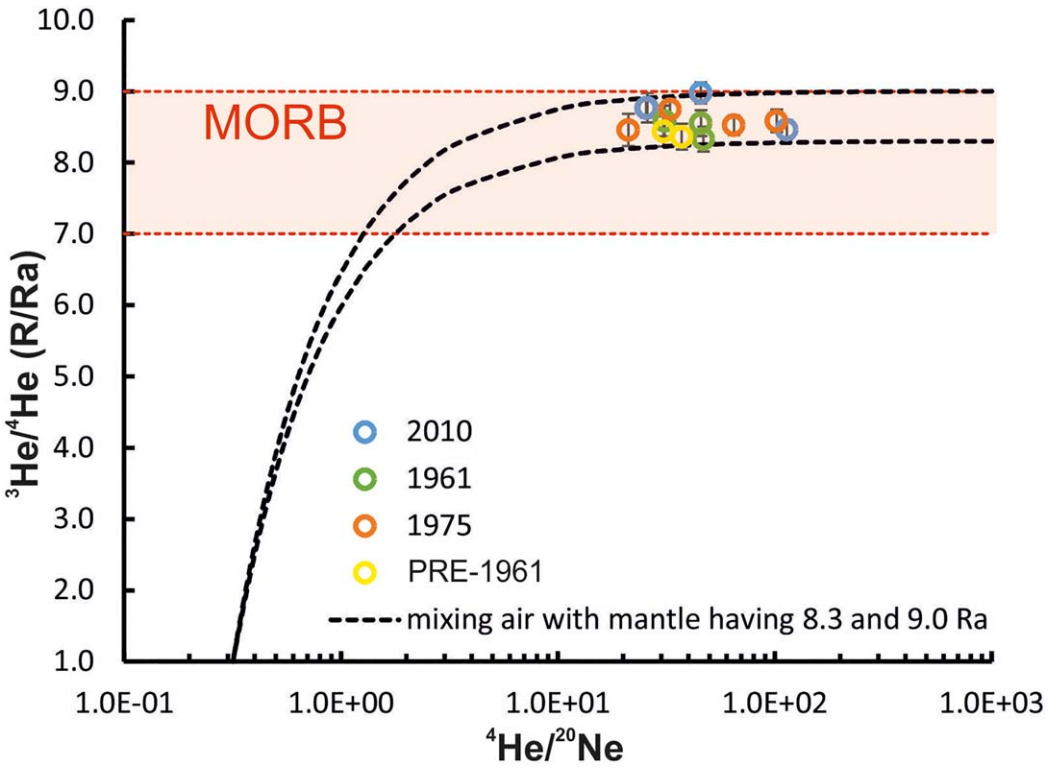

Figure 8. ^{3}He/^{4}He (expressed as R/Ra) versus ^{4}He/^{20}Ne for Pacaya olivine-hosted FIs (this work). The black lines reproduce the mixing curves between air and mantle with respectively 8.3 and 9.0 Ra. The MORB range is also indicated as in Figure 7.

1989). Excluding the highest value measured by Goff et al. (2000) (having a ^{3}He/^{4}He ratio of 7.9 Ra), the low ratios previously measured at Pacaya reasonably reflect the role of secondary processes, including air contamination or addition of radiogenic ^{4}He in the hydrothermal system.

5. Discussion

5.1. The Chemical Signature of Magmatic Gases at Pacaya

To the best of our knowledge, the only available volcanic gas composition for Pacaya was reported in (Goff et al., 2000) for 2 directly sampled fumaroles in 1992. Sano and Williams (1996) reported on δ^{13}C, R/Ra, $CO_2/^3$He information for one high-temperature Pacaya gas, but did not quote a complete gas analysis. The results of Goff et al. (2000) indicated a volcanic gas dominated by H_2O ($\sim$ 90 mol. %), CO_2 ($\sim$ 4–7 mol. %), and minor sulphur species. Unfortunately however, the low temperatures (84.5 and 342°C) and the high N_2 content (of the hottest sample) implied a non-trivial role of secondary processes, such as scrubbing of reactive volatiles by wall-rocks or hydrothermal fluids upon cooling, and mixing with atmospheric fluids (Fischer and Chiodini, 2015; Symonds et al., 2001). Our 2016 Multi-GAS results therefore, that were obtained on the summit crater plume directly released by a hot, erupting open-vent (Figure 2), provide the first assessment of the "magmatic" gas signature for Pacaya.

Our results (Table 1) suggest a variable gas composition during 14–22 January 2016 (Figures 4c and 4d). We find that the CO_2/SO_2 and H_2O/SO_2 ratios both varied widely, and that the two ratios were linearly correlated (Figure 9a). Using each couple of co-acquired ratios, we recalculate the molar proportions (in mol. %) of the three major volatiles in the magmatic gas phase. Validity of this procedure is based on the assumption that the above three species make together the totality of the source magmatic gas (a condition commonly encountered in volcanic gases; Fischer & Chiodini, 2015; Symonds et al., 1994). The derived compositions, shown in the triangular plot of Figure 9b, again show large variability, ranges being 38.4–96.8 mol. % (H_2O), 1.7–36.9 mol. % (CO_2) and 0.3–29.4 mol. % (SO_2).

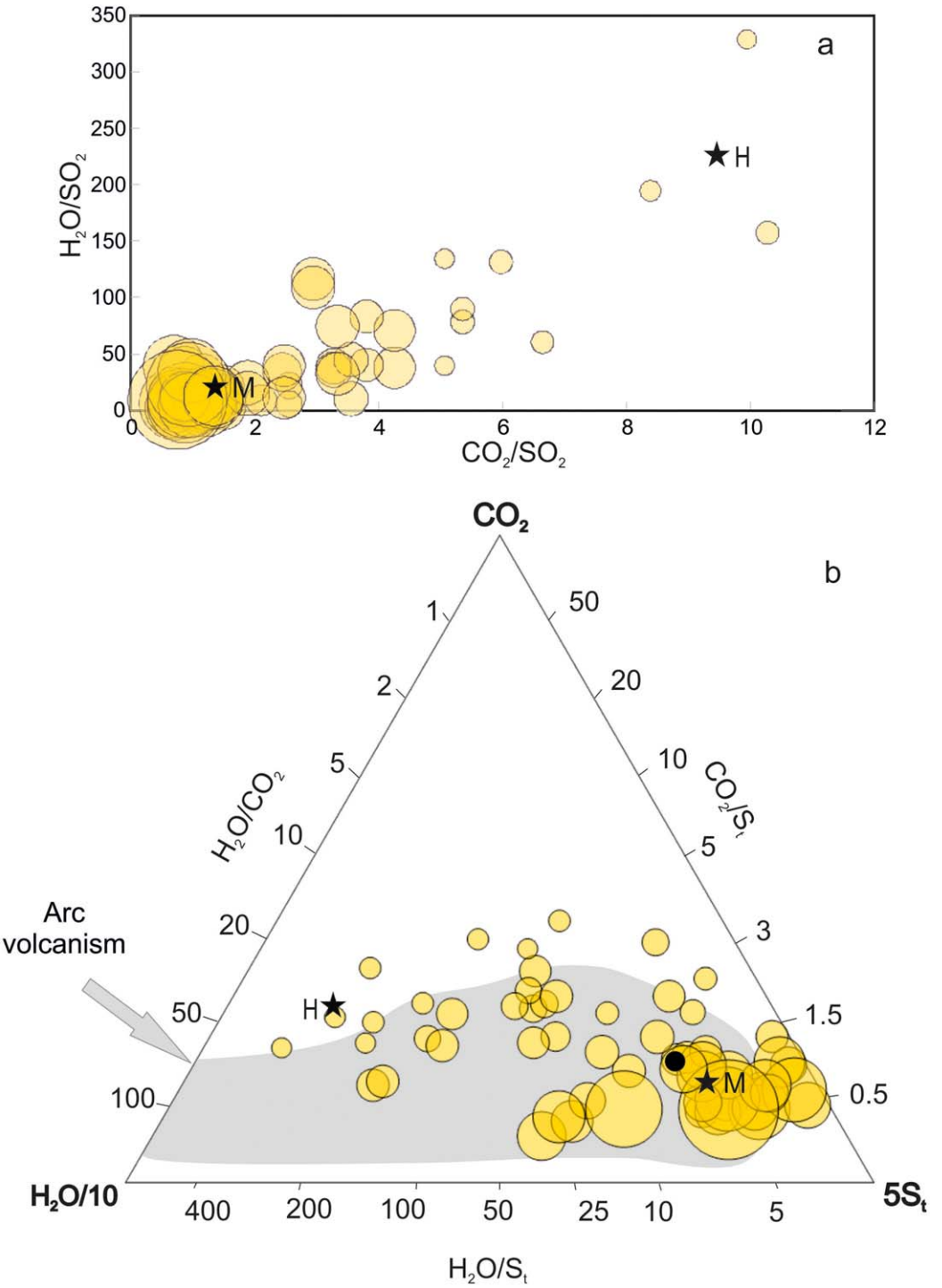

Figure 9. (a) H_2O/SO_2 versus CO_2/SO_2 scatter plot (data from Table 1); (b) $H_2O/10$-CO_2-$5S_t$ triangular plot, obtained from plume compositional data (of Table 1) recalculated to 100%. The grey background identifies the compositional range of volcanic arc gases globally (from Aiuppa, 2015). Data are interpreted as reflecting mixing of hydrothermal (H) and magmatic (M) end-member components. The composition of end-member H is fixed as the arithmetic mean of the three Multi-GAS data with highest CO_2/SO_2 (>8) and H_2O/SO_2 (> 150) ratios (see panel a)). The composition of the magmatic end-member M is the arithmetic mean of all Multi-GAS data with peak SO_2 concentrations > 20 ppm. The black circle in b) corresponds to composition of the Pacaya fumarole of Goff et al. (2000).

Several processes may have concurred to determine the observed compositional variability. One possibility is that the observed gas changes responded to variations in the volcano's degassing/activity state. However, strombolian intra-crateric activity and degassing both persisted at rather steady levels in the MacKenney crater during our study period. Except for a brief period in January 20–21, when strombolian activity was somewhat more vigorous, no major change was observed that could have explained the large diversity in gas composition. We instead propose that the observed gas variations reflected time-changing gas contributions from two distinct gas components, which we refer to as *H* and *M* (see Figure 9). Two-component mixing is fully supported by the linear compositional array in the ratio/ratio scatter plot of Figure 9a. We find that all gas compositions taken in high-SO_2 "dense plume conditions" were systematically characterized by low CO_2/SO_2 and H_2O/SO_2 ratios (Figures 4 and 9). Since SO_2 is commonly recognized as a tracer of high-temperature magmatic degassing (see reviews by Fischer & Chiodini, 2015; Oppenheimer et al., 2014), we conclude that the SO_2-rich, H_2O-CO_2-poor end-member composition *M* is likely to most closely approximate the Pacaya magmatic gas component. High CO_2/SO_2 and H_2O/SO_2 compositions were instead systematically observed when the plume sensed by the Multi-GAS was more dilute ($<$20 ppm SO_2; Figure 4). In analogy with observations made at other open-vent volcanoes (e.g., Etna; Shinohara et al., 2008), we propose that this low-SO_2 component (*H*) likely reflected gas contribution from lower temperature, hydrothermal fumaroles that were widespread on the crater rim/inner crater wall around the Multi-GAS site. Hydrothermal fumaroles are typically H_2O-rich (Chiodini & Marini, 1998; Fischer & Chiodini, 2015) and exhibit high CO_2/S_t ratios due to scrubbing of reactive sulfur during reactions with hydrothermal rocks/fluids (Aiuppa et al., 2014, 2017). The Pacaya fumaroles reported in Goff et al. (2000) may well be representative of this hydrothermal component.

Based on the above, we calculate our best-guess for the Pacaya magmatic gas composition by averaging all results taken in "dense plume" conditions (peak SO_2 concentration $>$ 20 ppm). We obtain a magmatic gas with 80.5 mol. % H_2O, 10.4 mol. % CO_2, and 9.0 mol. % SO_2, thus sitting at the H_2O-poor range of the population of volcanic arc gases worldwide (Aiuppa, 2015) (Figure 9b).

This unusual H_2O-poor gas composition could partially reflect our Multi-GAS measurements actually underestimating the real magmatic gas H_2O abundances, due to in-plume H_2O condensation during transport and dispersion, from the active degassing vent to the measurement site. Although we have no arguments to rule out this possibility completely, the Multi-GAS site was only 80 m distant from the vent, implying that a short-lived plume was actually measured (e.g., the transport time, from vent to the Multi-GAS, is inferred at $<$ 10 s, assuming a typical transport speed of 8.2 m/s). Alternatively, our results could imply a H_2O-poor magma source at Pacaya. Walker et al. (2003) analyzed a set of glass inclusions from the 1996–1999 activity of Pacaya, and found H_2O contents of $\approx$ 2 wt. % (range, 1.7-2.4). This is still within the normal range of H_2O abundances in arc magmas (Wallace, 2005; Wallace et al., 2015), but below (or, at least, at the lower range of) the observed glass inclusion H_2O contents in other Guatemalan volcanoes such as Agua (2.65-3.4), Atitlan (2.34-3.3), Fuego (up to 6 wt. %), and Santa Maria (1.5-3.5) (Roggensack, 2001; Sadofsky et al., 2008; Wehrmann et al., 2011). Based on these results, Walker et al. (2003) argued that the contribution of H_2O-rich slab fluids is likely more limited (0.1-0.3 wt. %) in the Pacaya mantle source region than underneath other Guatemalan volcanoes (0.5-0.7 wt. %). Clearly, additional near-vent gas observations, and possibly new glass inclusion data, are required to better confine the magmatic H_2O abundance at Pacaya.

5.2. Constraints on the Magmatic Source

Our inferred magmatic gas composition above implies a magmatic CO_2/S_t ratio for Pacaya of $\sim$1.1 ($\pm$ 1). This relatively low ratio, falling at the lower range of high-temperature arc volcanic gases worldwide (0.2–9.2; Aiuppa, 2015; Aiuppa et al., 2017), deserves some discussion. Recently, Aiuppa et al., (2014) analyzed the CO_2/S_t ratio signature of magmatic gases from the Costa Rica – Nicaragua segment (SNVS) of CAVA, and found distinct along-arc variations between its southern (Costa Rica, CO_2/S ratios: $\sim$0.5-1) and northern (Nicaragua; CO_2/S_t ratios: $\sim$3) branches. Based on positive correlations between magmatic gas CO_2/S_t ratios and trace-element tracers (e.g., Ba/La and U/Th) in the source magmas, Aiuppa et al. (2014, 2017) ascribed the increasing carbon-rich compositions in Nicaragua to the involvement of increasing proportions of recycled C-Ba-U-rich slab sediment fluids in magma genesis, compared to more mantle-like gas signature in Costa Rica.

Our novel results from Pacaya, with recent magmatic gas data from El Salvador (Aiuppa et al., 2017; Granieri et al., 2015), allow extending scrutiny of the gas versus trace element relation further to the north (Figure 10). Overall, these novel results corroborate the hypothesis of Aiuppa et al. (2014), indicating that, at the scale of the entire arc (CAVA), the linear correlation between gas CO_2/S_t ratios and Ba/La ratios (Figure 10a) is statistically significant ($R^2=0.7$), and follows the best-fit regression line:

$$CO_2/S_{t(m,\,gas)} = 0.03 \cdot \left(Ba/La_{m,rock}\right) + 0.07 \quad (3)$$

where $CO_2/S_{t(m,\ gas)}$ is the mean CO_2/S_t ratio in magmatic gases for each volcano (data from Aiuppa et al., 2014, 2017; Granieri et al., 2015); $(Ba/La_{m,rock})$ is the corresponding mean Ba/La ratio derived from published whole-rock analyses (extracted from the earthchem portal; http://www.earthchem.org/portal) and 0.03 and 0.07 are best-fit regression coefficients.

We find that the new Pacaya (and El Salvador) gas data allow filling the compositional gap between Central Costa Rica (e.g., Poas and Turrialba) and Nicaragua (Figure 10a). As such, these results are suggestive for the Pacaya magmatic gas having intermediate origin between mantle-like and slab-like end-member compositions in Costa Rica and Nicaragua, respectively. A higher mantle affinity of Pacaya magmas, relative to more sedimentary-derived signature of Nicaraguan magmas, is well consistent with available trace element and isotopic signatures of CAVA volcanites (Figure 10b; Carr & Feigenson, 1990; Leeman et al., 1994; Morris et al., 1990; Patino et al., 2000; Sadofsky et al., 2008), based on evidence from Cl isotopes, low U/Th ratios and $^{10}Be/^{9}Be$ in volcanic rocks, similarly suggested a slightly contaminated mantle source for Guatemala.

5.2.1. C and He Isotopes

Further and even clearer evidence on the mantle affinity of Pacaya magmas come from the $^{3}He/^{4}He$ ratios measured in fluid inclusions hosted in olivine crystals separated from the studied rocks. In fact, ^{3}He is typically mantle-sourced while ^{4}He is crustal and comes from the radiogenic decay of U and Th. This implies that strong contribution of mantle-derived gases can be detected in terms of strong increase of $^{3}He/^{4}He$ up to values higher than MORB range (i.e., >9 Ra), in case of lower mantle (i.e., plume) contribution (e.g., hot spot geodynamic setting). Our measured Rc/Ra vary between 8.3 and 9.0 Ra (Figure 7), which fall at the upper limit of MORB-like range ($R/Ra = 8 \pm 1$; Graham, 2002). More importantly, our $^{3}He/^{4}He$ ratios are the highest ever measured in CAVA and are among the highest ever recorded in arc volcanoes worldwide (Hilton et al., 2002; Oppenheimer et al., 2014, and references therein). Pacaya magmas thus point to a non-contaminated (by slab fluids) mantle wedge source beneath this segment of the volcanic arc, with no evidence of crustal contamination. According to Cameron et al. (2003), the southern portion of Guatemala undergoes E-W crustal extension, as evidenced by a series of N-S trending grabens (Burkart & Self, 1985). At Pacaya in particular, extensional regime is determined by the volcano laying at the intersection between the JFS and the Guatemala graben (Figure 1). Extensional forces are thought to control the degree of melting, and to facilitate rapid magma ascent, causing limited magma differentiation (Cameron et al., 2003). Modern Pacaya has erupted lavas of progressively more mafic composition, and uniquely basaltic rocks since historic time (Bardintzeff and Deniel, 1992). Another important aspect to consider is the role of decompression melting in south-eastern Guatemala. Cameron et al., (2003), based on major, trace elements and Sr isotopes in volcanic rocks, identified systematic differences between Pacaya and Agua (where decompression melting may play an important role) and other volcanoes in south-eastern Guatemala (i.e., Tecuamburro and Moyuta). They argued that Pacaya volcanics have compositions similar to back-arc cinder cones in southeastern Guatemala. These observations support the idea that the exceptionally high $^{3}He/^{4}He$ measured at Pacaya may reflect fast magma ascent from the mantle, limiting crustal contamination by radiogenic ^{4}He. Accordingly, the $^{3}He/^{4}He$ signature of the mantle wedge below this segment of Guatemala is not modified by subduction-related fluids.

The corrected $\delta^{13}C$ (CO_2) values of fumaroles sampled in this work are -3.5 and $-3.9‰$, respectively (cfr. 4.2). Considering the natural variability of the magmatic system, these values are comparable to the $\delta^{13}C$ values reported by Goff et al. (2000) (-2.8‰ and $-3.1‰$) for two fumaroles (at 84.5 and 342°C) sampled in the early 1990s. On the contrary, Sano and Williams (1996) reported a very low $\delta^{13}C$ (-6.9‰) for a high-temperature volcanic gas sample (965°C) from Pacaya. Because Sano and Williams (1996) did not report on the extent of air contamination of this sample, we cannot evaluate if the low $\delta^{13}C$ was the effect of a strong air dilution. In fact, a high extent of air contamination on a magmatic $\delta^{13}C$ of $-3‰$ would lead to more

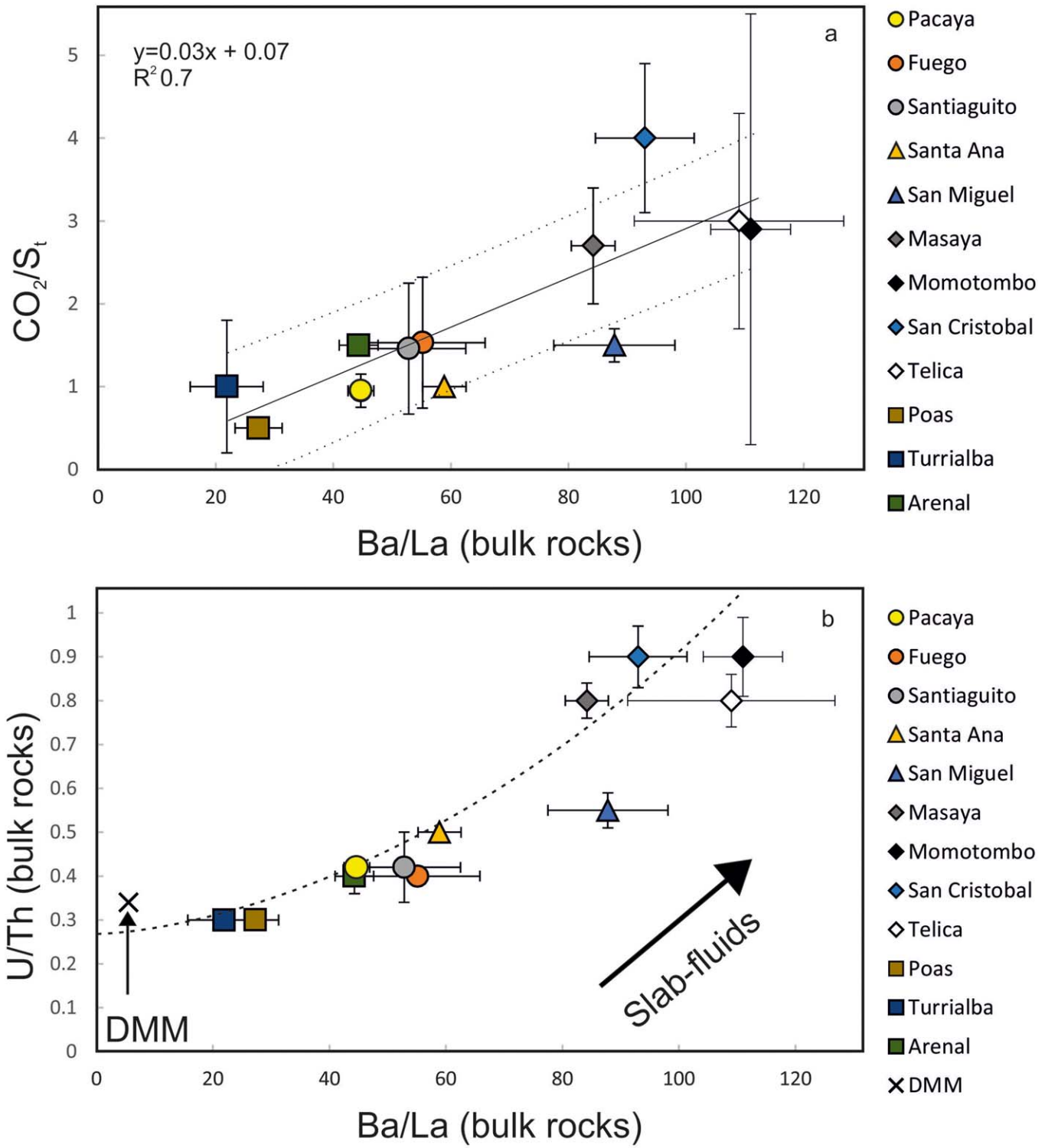

Figure 10. (a) Scatter plot of mean CO_2/S_t versus mean Ba/La and (b) mean U/Th versus mean Ba/La for CAVA volcanoes. For each volcano, the mean gas CO_2/S_t ratio is plotted, taken from this study (Pacaya) or from Aiuppa et al. (2014, 2017). The mean Ba/La and U/Th ratios were calculated averaging published whole-rock analyses (extracted from the earthchem portal; http://www.earthchem.org/portal). The error bars show one standard deviation. CO_2/S_t ratios for Fuego and Santiaguito are derived from equation (3) using available Ba/La information (from earthchem portal). The dashed lines in (a) represent the confidence intervals ($\pm$ 0.75 at 1 σ) on the estimated CO_2/S_t ratios. DMM is the composition of Depleted MORB Mantle source (Salters & Stracke, 2004).

negative ratios (air $\delta^{13}C$=-8‰). Alternatively, their low $\delta^{13}C$ (CO_2) could reflect a residual (degassed) magmatic source (see below). As detailed below, $\delta^{13}C$ of CO_2 may suffer an isotope fractionation during magmatic degassing that leads to more negative ratios. For the above reasons, we discarded this low ratio, and we hereafter assume an average $\delta^{13}C = -3.5 \pm 0.4$‰ as representative of the magmatic signature of carbon at Pacaya. We caution that, in contrast to $^3He/^4He$ ratios that can be directly used to constrain the origin of fluids, $^{13}C/^{12}C$ ratios are more problematic to interpret, owing to the existence of isotopic fractionations during magmatic degassing and gas-water interactions. Experiments demonstrate that, in basaltic melts, C isotopes have vapour-melt enrichment factors ($\varepsilon_{CO2\text{-}melt}$) of 2 to 4‰, e.g., ^{13}C is preferentially extracted from melt. Because of this, the $\delta^{13}C$ signature of magmatic CO_2 decreases along both open- and closed-system magma degassing paths (Javoy et al., 1978; Mattey, 1991; Trull et al., 1993). Unfortunately, no independent constraint is available at Pacaya to quantify the degassing extent of the magma source feeding our Pacaya fumaroles. In addition, a possible gas-water-rock interaction control on $\delta^{13}C$ (and $CO_2/^3He$) cannot be ruled out in our Pacaya example, in view of the low fumarole temperatures (at which scrubbing is important; Symonds et al., 2001). It follows from the above that caution is needed when interpreting $\delta^{13}C$ and $CO_2/^3He$ variations at any single volcano or along an arc segment. These tracers may not necessarily provide direct access to the relative slab versus mantle contributions to magmatism (Sano & Marty, 1995). In the limit-case assumption that secondary processes are negligible, the magmatic signature in the gaseous phase of Pacaya melts would have $\delta^{13}C$ of -3.5 ± 0.4‰. This is in the range of MORB-like mantle, whose inferred $\delta^{13}C$ range is between −8‰ and −4‰ (Deines, 2002; Javoy & Pineau, 1991; Macpherson & Mattey, 1994; Marty & Jambon, 1987; Sano & Marty, 1995).

In order to put our novel $^3He/^4He$-$\delta^{13}C$ results in the context of CAVA (Figure 11), we need to make some general considerations on data selection. Detailed $^3He/^4He$-$\delta^{13}C$ data sets are available for CAVA in

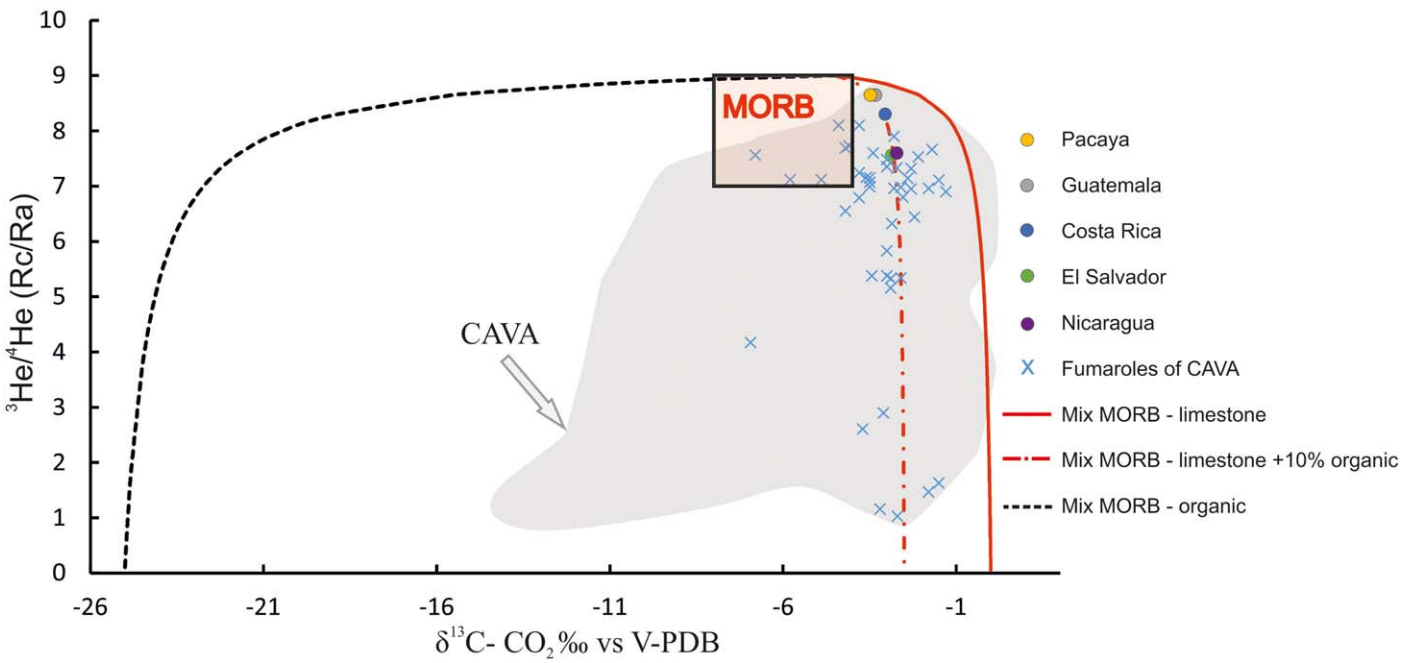

Figure 11. Plot of $\delta^{13}C$ of CO_2 versus $^3He/^4He$ ratio in CAVA volcanic gas samples. Colored circles represent average compositions for Pacaya and for the different CAVA volcanic arc segments. For each CAVA volcano that contributed to calculation of the averaged CAVA segment values, we considered the maximum Rc/Ra values measured in fumarole gases and FIs (where available), and the mean $\delta^{13}C$ of crater fumaroles only (see text for further details). See Table 4 for data sources. The blue crosses are compositions of individual fumarolic gas samples from CAVA (including low- and high-temperature fumaroles). The grey shaded area identifies the whole CAVA gas compositional field (including data from springs, flank fumaroles, peripheral gases; modified from Oppenheimer et al. (2014), see the original work for data sources). The $\delta^{13}C$ of CO_2 for Pacaya is an average on data from this work and those reported by Goff et al. (2000) (-2.8‰ and −3.1‰) for two fumaroles (at 84.5 and 342°C) sampled in the early 1990s. Details are reported in the Table 4. The red solid line represents mixing between MORB ($\delta^{13}C$= −4.5‰, Rc/Ra=9, $CO_2/^3He$=2E+9) and limestones ($\delta^{13}C$=0‰, Rc/Ra =0.05, $CO_2/^3He$ =1E+13) (end-members taken from Sano and Marty (1995), and Graham (2002)). The black dashed line depicts mixing between MORB and organic carbon having $\delta^{13}C$=-25‰, Rc/Ra = 0.05, $CO_2/_3He$ = 1E + 13 (Sano & Marty, 1995). The red dashed line corresponds to mixing between MORB and limestones plus addition of 10% organic carbon.

comparison to other arc segments (e.g., Fischer et al., 2007; Hilton et al., 2002; Oppenheimer et al., 2014, and references therein). However, the measured range is large for both $^3He/^4He$ (0.7–8.1 Ra) and $\delta^{13}C$ (from $-14‰$ to $0‰$). Large He and C variations are observed not only among different CAVA volcanoes, but also within the same volcanic system (Fischer et al., 2007). This variability is largely an effect of the disparate use of different gas (high- and low-temperature crater fumaroles, flank gases, geothermal springs, and distal gas emissions) and sample (FIs in olivine phenocrysts versus gas emissions) types. In the majority of CAVA volcanoes analyzed so far (Di Piazza et al., 2015; Fischer et al., 2005; Robidoux et al., 2017; Shaw et al., 2006), the $^3He/^4He$ ratios in olivine-hosted fluid inclusions are typically higher than in (or at the upper range of) volcanic gases from the same volcanic system. FIs should thus be prioritized as more reliable indicators of the magmatic/mantle signature, where available. $^{13}C/^{12}C$ ratios are currently difficult to measure in olivine-hosted fluid inclusions, except in mantle xenoliths or in phenocrysts crystallized at high depth (Correale et al., 2015; Deines, 2002; Gennaro et al., 2017). Thus, volcanic gases remain in most cases the only source of information, but should be limited to sample types showing greater magmatic affinity (e.g., high-temperature crater fumaroles should be preferred to hydrothermal or distal gas emissions).

In view of the above, our selected CAVA $^3He/^4He$-$\delta^{13}C$ population includes, for each volcano, the maximum Rc/Ra values measured (in FIs where available), and the mean $\delta^{13}C$ of crater fumaroles only (Figure 11). This selected CAVA subset (Table 4) gives the opportunity to make some considerations on along-arc variations of these tracers. Before our study, the highest $^3He/^4He$ values along CAVA had been measured at Turrialba (Costa Rica), with values up to 8.1 Ra in fumarole gases (Di Piazza et al., 2015; Hilton et al., 2010; Shaw et al., 2003; Tassi et al., 2004; Vaselli et al., 2010) and up to 8.3 Ra in fluid inclusions in olivines (Di Piazza et al., 2015; Fischer et al., 2005; Shaw et al., 2006). Slightly lower ratios (up to 7.6 Ra; Fischer et al., 2015; Hilton et al., 2010; Poreda & Craig, 1989; Shaw et al., 2003), but still within the MORB range, have also been measured in crater fumaroles from the nearby Póas volcano (Fischer et al., 2015; Hilton et al., 2010; Sano & Williams, 1996; Shaw et al., 2003) (Figure 11). These high ratios have widely been interpreted as representative of the signature of the mantle wedge beneath this segment of CAVA, with no (or very limited) contribution

Table 4
Geochemical Tracers, Isotopic Carbon Composition and Rc/Ra for Selected Sub-data set of CAVA Segment

Volcano	U/Th	Ba/La	$CO_2/^3He$	$\delta^{13}C‰$	Rc/Ra
Pacaya	0.45	44	1.89E+10[a,b]	−3.46[a,c]	8.65[c,d]
Tecuamburro				−3.0[e]	5.96[e]
Zunil			1.14e+10[b]	−2.86[b]	6.32[b]
Guatemala	**0.45**	**44**	**1.89E+10[a,b]**	**−3.33[b]**	**8.65[c]**
Santa Ana	0.50	60	2.07E+10[f]	−2.55[f]	7.56[f,g]
El Salvador	**0.50**	**60**	**2 .07E+10**	**−2.55[f]**	**7.56[f]**
Masaya	0.80	85	2.30E+10[h]	−1.50[h]	7.23[g,h]
Cerro Negro	0.84	118.71	2.01E+10	−2.72[b,i]	7.38[g,i]
Momotombo	0.90	110	2.70E+10[h]	−2.60[h,j]	7.40[d,h]
Mombacho	0.67	59.19	1.78E+10[h]	−3.25[h]	7.60[g,h]
San Cristobal	0.90	90	3.20E+10[h]	−2.95[h]	7.20[d,j]
Nicaragua	**0.82**	**92.58**	**2.40E+10[h]**	**−2.60[b,i]**	**7.60[h]**
Poas	0.30	26	2.02E+10[k,l]	−3.54[b,l]	7.60[k,l]
Turrialba	0.30	20	1.41E+10[h,n]	−3.01[h,n]	8.30[d,m]
Costa Rica	**0.30**	**23.00**	**1.72E+10[h,n]**	**−3.27[h,n]**	**8.30[g,m]**
DMM	0.35	7	2.00E+09[o]	−4.50[o]	8 ± 1 Ra[p]
Organic carbon			1.00E+13	−25	0.05
Carbonate sediments	1.63	244.36	1.00E+13	0	0.05

Note. U/Th and Ba/La ratios are average whole-rock values calculated from rock compositions extracted from the earthchem portal (http://www.earthchem.org/portal). See also Aiuppa et al. (2014) for reference (Uncertainties in the mean values are given as error bars in Figure 10). $CO_2/^3He$ and $\delta^{13}C$ are mean of fumaroles reported in Figure 11 as blue x symbol. Rc/Ra are air-corrected $^3He/^4He$ ratios normalized to the atmospheric $^3He/^4He$ ratio (Ra). The maximum value measured in each volcanic system is reported (except for end-members).

[a]Goff et al., (2000). [b]Sano and Williams (1995). [c]This work. [d]Fluid inclusion. [e]Janik et al. (1992). [f]Leeuw et al. (2007). [g]Fumaroles. Average values for nations are the same reported in Figure 11. [h]Shaw et al. (2006). [i]Lucic et al. (2014). Allard (1983). [j]Robidoux et al. (2017). [k]Fisher et al. (2015). [l]Hilton et al. (2002). [m]Tassi et al. (2004). [n]Vaselli et al. (2010). [o]Sano and Marty (1996). [p]Graham (2002).

from the subducting Cocos plate lithosphere. This MORB affinity of Costa Rican volcanism is supported by several independent geochemical indicators such as the low Ba/La, Ba/Th, and U/Th ratios in the erupted rocks (Patino et al., 2000; Sadofsky et al., 2008). The few measurements carried out in El Salvador at Santa Ana volcano gave a $^3He/^4He$ up to 7.6 Ra (de Leeuw et al., 2007), while in Nicaragua the $^3He/^4He$ ration ranged from 7.2 Ra at San Cristobal (Robidoux et al., 2017) to 7.6 at Mombacho (Shaw et al., 2003) (Figure 11). In consideration of the high $^3He/^4He$ we measured at Pacaya, Figure 11 strongly reinforces the hypothesis of a mantle signature with no appreciable addition of radiogenic ^4He from the slab or the crust in SE-Guatemala, similar to Southern Costa Rica. The increased sediment input from the subducting slab beneath Nicaraguan segment of CAVA, highlighted by high Ba/La and U/Th ratios (Sadofsky et al., 2008), only leads to a minor decline of the $^3He/^4He$ ratio.

As for $\delta^{13}C$ (Table 4 and Figure 11), the Pacaya $\delta^{13}C$ signature (-3.5 $\pm$ 0.4‰) approaches the average isotope compositions of Costa Rican ($\delta^{13}C$ -3.1 ± 1.3; Fischer et al., 2015; Hilton et al., 2010; Sano & Williams, 1996; Shaw et al., 2003; Tassi et al., 2004; Vaselli et al., 2010) and Guatemalan ($\delta^{13}C = -3.3 \pm 0.4$‰; Goff et al., 2000; Janik et al., 1992; Sano & Williams, 1996; this work) volcanoes, and reflect high mantle contributions. Slightly more positive signatures are observed in El Salvador and Nicaragua ($\delta^{13}C = -2.9 \pm 0.6$‰ and -2.7 ± 0.6‰, respectively; Allard, 1983; Sano & Williams, 1996; Shaw et al., 2003; Snyder et al., 2001) that could be compatible with an enhanced limestone contribution ($\delta^{13}C = 0$‰; Sano & Marty, 1995) with possible addition of organic carbon up to 10% in the central CAVA segment. This is shown in Figure 11 by the dashed mixing curve, which supports the hypothesis that this is a mantle feature of the subducting slab common to most of the volcanoes of CAVA.

5.3. Volatile Fluxes

Our results also set the basis for a first assessment of the total volatile flux from Pacaya. Our measured SO_2 flux on 16 January 2016 was 885 $\pm$ 550 tons/d (Figure 5c), thus falling in the middle of previously reported SO_2 fluxes for the volcano. These have fluctuated substantially since onset of the ongoing eruptive period in 1965. Published SO_2 fluxes have remained at low levels in the 1970s–1990s, from 260 tons/day (1973–1993 mean; Andres et al., 1993) to 510 tons/day (1972–1997 mean; Andres & Kasgnoc, 1998). They then apparently peaked at 1,350–1,540 in the 1999–2002 period (GVN Bullettin, 2002; Mather et al., 2006; Rodríguez et al., 2004), to decrease again in the mid- to late-2000s, from 270–400 tons/day (in 2004–2005; Bluth et al., 2007) to <120 tons/day (in 2008; Dalton et al., 2010). Our 2016 data therefore suggest intensification of degassing activity relative to the low fluxes seen in the most recent (2004–2008) published reports.

We combine our SO_2 flux results with the above best-guess for the Pacaya magmatic gas composition (80.5 mol. % H_2O, 10.4 mol. % CO_2, and 9.0 mol. % SO_2) to infer the H_2O and CO_2 fluxes for Pacaya for the first time. So doing, our SO_2 fluxes and compositions convert into H_2O and CO_2 fluxes of 2,230 $\pm$ 1,390 and 700 $\pm$ 440 tons/day for 16 January 2016. The large associated uncertainties reflect the huge temporal variability of SO_2 fluxes (62% variation at 1 SD) during our measurement interval, and underscore for the need of longer, more systematic observations to better constrain the volcano's degassing strength. We also infer a H_2 flux of $\sim$1.1 $\pm$ 0.7 tons/day based on a H_2/SO_2 of 0.04 $\pm$ 0.01. Based on our results, the Total Volatile Flux in January 2016 was $\sim$3,800 $\pm$ 2,375 tons/d (Table 5), ranking Pacaya as a medium volcanic arc emitter. For example, our measured CO_2 flux ranks Pacaya at #18 in the list of the #44 volcanoes for which CO_2 information is available (Aiuppa, 2015; Burton et al., 2013).

Table 5
Volatile Fluxes on 16 January 2016

	mol %	Flux (tons/d)
H_2O	80.5	2,230 $\pm$ 1,390[b]
CO_2	10.4	700 $\pm$ 440[b]
SO_2	9.0	885 $\pm$ 550[a]
H_2	0.1	1.1 $\pm$ 0.7[b]
Total Volatile flux[c]	100	3,800 $\pm$ 2,375

[a]From UV camera, data from Figure 5. [b]Calculated scaling the each X/SO_2 ratio by the mean SO_2 flux. [c]Sum of H_2O, CO_2, SO_2 and H_2 fluxes.

5.4. Implications for the Volcanic CO_2 Output in Guatemala

We use our novel results for Pacaya to attempt at a preliminary characterization of the CO_2 output from the Guatemalan segment of CAVA. Refining the arc CO_2 output, both globally and at the scale of individual arc segments, is mandatory for better constraining the CO_2 arc budget, e.g., to infer the fraction of subducted carbon (with slab sediments and altered oceanic crust) that is recycled via volcanic arc magmatism and, by difference, the fraction transported back into the deep mantle (Dasgupta, 2013; Kelemen & Manning, 2015). Owing to the lack of magmatic gas data, the Guatemalan contribution to the CAVA CO_2 output has only been indirectly established in past studies,

by using either gas information from other, better studied segments of the arc (e.g., Hilton et al., 2002), or a "mean arc gas CO_2/SO_2 ratio" proxy (Mather et al., 2006).

In addition to Pacaya, Fuego and Santiaguito (Figure 1) are the two other Guatemalan volcanoes showing sustained, persistent degassing activity (Rodríguez et al., 2004). In the classic SO_2 flux compilation study of Andres and Kasgnoc (1998), the two volcanoes had reported time-averaged (1972–1997 period) SO_2 emissions of 640 and 230 tons/day, respectively. For comparison, Rodríguez et al. (2004) reported SO_2 flux data for the 1999–2002 period being twice as low (337 ± 145 and 127 ± 58 tons/day, respectively). These data confirm Pacaya as the strongest degassing source in Guatemala, but also imply a not trivial CO_2 contribution from Fuego and Santiaguito.

The volcanic gas CO_2/SO_2 ratio signature and the CO_2 output are unfortunately undetermined for Fuego and Santiaguito. However, plenty of whole-rock information is available for magmas erupted at both volcanoes. Importantly, trace-element co-variation diagrams (e.g., Figure 10b) suggest magmas erupted at Fuego and Santiaguito plot along the same compositional array of other CAVA magmas (Sadofsky et al., 2008, and references cited therein). This opens the possibility to estimate the magmatic gas CO_2/SO_2 ratio signature of Fuego and Santiaguito based on the CAVA gas (CO_2/S_t ratio) versus trace-element (Ba/La ratio) relationship of Figure 10a. Using equation (3), and with the specific $Ba/La_{m,rock}$ derived in earthchem for each volcano (Fuego: 55.1 ± 10.6; Santiaguito: 52.8 ± 9.7), we derive $CO_2/S_{t(m,\ gas)}$ ratios of respectively 1.5 ± 0.75 and 1.4 ± 0.75. Here, the confidence interval or delta (± 0.75), calculated from the regression line and one standard deviation (Figure 10a), is taken as a proxy for the uncertainty in predicted $CO_2/S_{t(m,\ gas)}$ ratios.

We caution the above procedure is likely to provide only a rough approximation of the real magmatic gas CO_2/S_t ratio for each volcano, and that direct volcanic gas observations remain needed here. Yet, we can use our predicted CO_2/S_t ratios above (1.5 ± 0.75 and 1.4 ± 0.75) in tandem with time-averaged SO_2 fluxes (337 ± 145 and 127 ± 58 tons/day, respectively), to preliminary evaluate the CO_2 flux at respectively 347 ± 375 (Fuego) and 122 ± 121 (Santiaguito). With these numbers, and considering the Pacaya CO_2 flux determined above, the total volcanic CO_2 flux from Guatemala would be ~1,160 ± 600 tons/d. This would respond to ~30% of the CO_2 flux from the Costa Rica – Nicaragua Volcanic Segment (CNSV: 2,835–3,184 tons/d, (Aiuppa et al., 2014), and ~16% of the total CAVA output (~6,932 tons/d; Hilton et al., 2002).

6. Conclusions

We have here investigated (i) the composition of the volcanic gas plume released by Pacaya volcano in Guatemala, and (ii) the noble gas composition of FIs trapped in olivines separated from rocks of some of the volcano's most recent eruptions. This novel data set is used to characterize the magmatic gas signature and the Total Volatile Flux budget for one of the most active CAVA volcanoes for the first time.

Our plume compositional data suggest Pacaya exhibits a H_2O-poor (for an arc volcano) composition (80.5 mol. %), with a characteristic magmatic CO_2/S_t ratio of ~1.0 to 1.5. Both the H_2O-poor and low CO_2/S_t ratio composition concur to suggest a limited slab-fluid contribution (at least compared to other volcanoes/arc segments; Aiuppa et al., 2017), and a dominant mantle-wedge derivation of the emitted volatiles. The $^3He/^4He$ ratios measured in fluid inclusions hosted in olivines (Ra) are within the MORB range (8 ± 1Ra) and among the highest values in CAVA volcanism. This strongly supports that the mantle source beneath Pacaya lacks of any contamination of radiogenic ^4He from the slab or the crust, as observed in Costa Rica segment of CAVA. This mantle affinity for He (and C) is consistent with independent petrological/geochemical evidence for magmas underneath Pacaya forming by decompressional melting rather than by slab-fluid addition, and also points to rapid magma transit in the crust, favored by local extensional regime.

We have also estimated the Pacaya Total Volatile Flux at ~3,800 tons/d in January 2016, a period of relatively mild intra-crateric strombolian activity. The Pacaya CO_2 flux accounts at 700 ± 440 tons/day (16 January 2016), implying the volcano is a moderate volcanic arc CO_2 emitter. By combining this measured Pacaya CO_2 flux with inferred CO_2 fluxes from Fuego and Santiaguito (using the CAVA CO_2/S_t ratio versus Ba/La ratio association), we tentatively assess the total volcanic CO_2 flux from Guatemalan segment of CAVA at ~1,160 tons/d.

Acknowledgments
This research received funding from the Deep Carbon Observatory Deep Earth Carbon Degassing program and from the European Research Council (FP7/ERC grant agreement n. 305377). We wish to thank Dulce María Esther González Domínguez for help during rocks sampling, Philippe Robidoux and Andrea Di Piazza for mineral preparation as well as Manuela Nazzari for EMPA measurements at INGV, Sezione di Roma 1. We are also grateful to Mariano Tantillo and Mariagrazia Misseri for their support in sample preparation and noble gases analysis of fluid inclusions. We finally thank Mauro Martelli and Francesco Salerno for chemical composition of fumaroles as well as Fausto Grassa, Ygor Oliveri and Aldo Sollami for the following carbon isotopes measures. Comments by the Associate Editor (T. Fischer) and two anonymous Reviewers improved the manuscript. All the data used for this paper are available in the Tables reported in the text (Tables (1–5)) and in supporting information (S1–S4) and by contacting the corresponding author.

References

Aiuppa, A., Bani, P., Moussallam, Y., Di Napoli, R., Allard, P., Gunawan, H., et al. (2015). First determination of magma-derived gas emissions from Bromo volcano, eastern Java (Indonesia). *Journal of Volcanology and Geothermal Research*, *304*, 206–213.

Aiuppa, A., Federico, C., Giudice, G., & Gurrieri, S. (2005). Chemical mapping of a fumarolic field: La Fossa Crater, Vulcano Island (Aeolian Islands, Italy). *Geophysical Research Letters*, *32*, L13309. https://doi.org/10.1029/2005GL023207

Aiuppa, A., Fischer, T. P., Plank, T., Robidoux, P., & Di Napoli, R. (2017). Along-arc, inter-arc and arc-to-arc variations in volcanic gas CO2/ST ratios reveal dual source of carbon in arc volcanism. *Earth-Science Reviews*, *168*, 24–47. https://doi.org/10.1016/j.earscirev.2017.03.005

Aiuppa, A., Robidoux, P., Tamburello, G., Conde, V., Galle, B., Avard, G., et al. (2014). Gas measurements from the Costa Rica-Nicaragua volcanic segment suggest possible along-arc variations in volcanic gas chemistry. *Earth Planetary Science Letters*, *407*, 134–147.

Allard, P. (1983). The origin of hydrogen, carbon, sulfur, nitrogen, and rare gases in volcanic exhalations: Evidence from isotope geochemistry. In H. Tazieff & J.-C. Sabroux (Eds.), *Forecasting volcanic events* (pp. 337–386). Amsterdam, The Netherlands: Elsevier.

Andres, R. J., & Kasgnoc , A. D. (1998). A time-averaged inventory of subaerial volcanic sulfur emissions. *Journal of Geophysical Research*, *103*(D19), 25251–25261.

Andres, R. J., Rose, W. I., Stoiber, R. E., Williams, S. N., Matías, O., & Morales, R. (1993). A Summary of Sulfur dioxide emission rate measurements from Guatemalan volcanoes. *Bulletin of Volcanology*, *55*(5), 379–388.

Bardintzeff, J.-M., & Deniel, C. (1992). Magmatic evolution of Pacaya and cerro Chiquito volcanological complex, Guatemala. *Bulletin of Volcanology*, *54*(4), 267–283.

Barnes, J. D., Sharp, Z. D., Fischer, T. P., Hilton, D. R., & Carr, M. J. (2009). Chlorine isotope variations along the Central American volcanic front and back arc. *Geochemistry, Geophysics, Geosystems*, *10*, Q11S17. https://doi.org/10.1029/2009GC002587

Bluth, G. J. S., Shannon, J. M., Watson, I. M., Prata, A. J., & Realmuto, V. J. (2007). Development of an ultra-violet digital camera for volcanic SO2 imaging. *Journal of Volcanology and Geothermal Research*, *161*(1–2), 47–56.

Burkart, B., & Self, S. (1985). Extension and rotation of crustal blocks in northern Central America and effect on the volcanic arc. *Geology*, *13*, 22–26.

Burton, M. R., Oppenheimer, C., Horrocks, L. A., & Francis , P. W. (2000). Remote sensing of CO2 and H2O emission rates from Masaya volcano, Nicaragua. *Geology*, *28*(10), 915–918.

Burton, M. R., Sawyer, G. M., & Granieri, D. (2013). deep Carbon Emission from Volcanoes. *Reviews in Mineralogy & Geochemistry*, *75*(1), 323–354. https://doi.org/10.2138/rmg.2013.75.11

Cameron, B. I., Walker, J. A., Carr, M. J., Patino, L. C., Matías, O., & Feigenson, M. D. (2003). Flux versus decompression melting at stratovolcanoes in southeastern Guatemala. *Journal of Volcanology and Geothermal Research*, *119*((1–4), 21–50.

Carr, M. J. (1984). Symmetrical and segmented variation of physical and geochemical characteristics of the Central American volcanic front. *Journal of Volcanology and Geothermal Research*, *20*(3–4), 231–252.

Carr, M. J., & Feigenson, M. D., & Bennett, E. A. (1990). Incompatible element and isotopic evidence for tectonic control of source mixing and melt extraction along the Central American arc. *Contribution to Mineralogy and Petrology*, *105*(4), 369–380.

Case, J. E., MacDonald, W. D., & Fox, P. J. (1990). Caribbean crustal provinces; seismic and gravity evidence. In G. Dengo & J. E. Ž. Case (Eds.), *The Caribbean Region: The Geology of North America* (Vol. H, pp. 15–36). Boulder, CO: Geological Society of America. https://doi.org/10.1130/DNAG-GNA-H

Chan, L. H., Leeman, W. P., & You, C. F. (2002). Lithium isotopic composition of Central American volcanic arc lavas: Implications for modification of subarc mantle by slab-derived fluids: Correction. *Chemical Geology*, *182*(2–4), 293–300. https://doi.org/10.1016/S0009-2541(01)00298-4

Chiodini, G., & Marini, L. (1998). Hydrothermal gas equilibria: The H2O-H2-CO2-CO-CH4 system. *Geochimica et Cosmochimica Acta*, *62*, 2673–2687.

Conde, V., Robidoux, P., Avard, G., Galle, B., Aiuppa, A., Muñoz, A., & Giudice, G. (2014). Measurements of volcanic SO_2 and CO_2 fluxes by combined DOAS, Multi-GAS and FTIR observations: A case study from Turrialba and Telica volcanoes. *International Journal of Earth Sciences*, *103*(8), 2335–2347.

Conway, F. M., Diehl, J. F., & Matías, O. (1992). Paleomagnetic constraints on eruption patterns at the Pacaya composite volcano, Guatemala. *Bulletin of Volcanology*, *55*(1–2), 25–32.

Correale, A., Paonita, A., Rizzo, A., Grassa, F., & Martelli , M. (2015). The carbon-isotope signature of ultramafic xenoliths from the Hyblean Plateau (southeast Sicily, Italy): Evidence of mantle heterogeneity. *Geochemistry, Geophysics, Geosystems*, *16*, 600–611. https://doi.org/10.1002/2014GC005656

D'Aleo, R., Bitetto, M., Delle Donne, D., Tamburello, G., Battaglia, A., Coltelli, M., et al. (2016). Spatially resolved SO_2 flux emission from Mt Etna. *Geophysical Research Letters*, *43*, 7511–7519. https://doi.org/10.1002/2016GL069938

Dalton, M. P., Waite, G. P., Watson, I. M., & Nadeau, P. A. (2010). Multiparameter quantification of gas release during weak Strombolian eruptions at Pacaya Volcano, Guatemala. *Geophysical Research Letters*, *37*, L09303. https://doi.org/10.1029/2010GL042617

Dasgupta, R. (2013). Ingassing, storage, and outgassing of terrestrial carbon through geologic time. *Reviews in Mineralogy & Geochemistry*, *75* (1), 183–229.

Deines, P. (2002). The carbon isotope geochemistry of mantle xenoliths. *Earth-Science Reviews*, *58*(3–4), 247–278. https://doi.org/10.1016/S0012-8252(02)00064-8

De Leeuw, G. A. M., Hilton, D. R., Fischer, T. P., & Walker, J. A. (2007). The He–CO2 isotope and relative abundance characteristics of geothermal fluids in El Salvador and Honduras: New constraints on volatile mass balance of the Central American Volcanic Arc. *Earth and Planetary Science Letters* , *258*(1–2), 132–146.

de Moor, J. M., Aiuppa, A., Avard, G., Wehrmann, H., Dunbar, N., Muller, C., et al. (2016). Turmoil at Turrialba Volcano (Costa Rica): Degassing and eruptive processes inferred from high-frequency gas monitoring. *Journal of Geophysical Research: Solid Earth*, 121, 5761–5775, https://doi.org/10.1002/2016JB013150

DeMets , C. (2001). A new estimate for present- day Cocos-Caribbean plate motion: Implication for slip along the Central American volcanic arc. *Geophysical Research Letters*, *28*(21), 4043–4047.

de Moor, J. M., Kern, C., Avard, G., Muller, C., Aiuppa, A., Saballos, A., et al. (2017). A new sulfur and carbon degassing inventory for the Southern Central American Volcanic Arc: The importance of accurate time-series data sets and possible tectonic processes responsible for temporal variations in arc-scale volatile emissions. *Geochemistry, Geophysics, Geosystems*, *18*, 4437–4468. https://doi.org/10.1002/2017GC007141

Di Piazza, A., Rizzo, A. L., Barberi, F., Carapezza, M. L., De Astis, G., Romano, C., & Sortino, F. (2015). Geochemistry of the mantle source and magma feeding system beneath Turrialba volcano, Costa Rica. *Lithos*, *232*, 319–335.

Eggers A. A. (1971), *The geology and petrology of the Amatitlán quadrangle, Guatemala* (Ph. D. dissertation, 221 p.). Hanover, NH: Dartmouth College.

Feigenson, M. D., & Carr, M. J. (1986). Positively correlated Nd and Sr isotope ratios of lavas from the Central American volcanic front . *Geology*, *14*(1), 79–82. https://doi.org/10.1130/0091-7613(1986)14 < 79:PCNASI>2.0.CO;2

Fischer, T. P., & Chiodini, G. (2015). Volcanic, magmatic and hydrothermal gases. In Sigurdsson, H., et al. (Eds.), *The encyclopedia of volcanoes* (2nd ed., pp. 779–797). San Diego, CL: Elsevier Inc. https://doi.org/10.1016/B978-0-12-385938-9.00045-6

Fischer, T. P., Hilton, D. R., Zimmer, M. M., Shaw, A. M., Sharp, Z. D., & Walker, J. A. (2002). Subduction and recycling of nitrogen along the Central American Margin. *Science*, *297*(5584), 1154–1157.

Fischer, T. P., & Marty, B. (2005). Volatile abundances in the sub-arc mantle: Insights from volcanic and hydrothermal gas discharges. *Journal of Volcanology and Geothermal Research*, *140*(1–3), 205–216.

Fischer, T. P., Ramírez, C., Mora-Amador, R. A., Hilton, D. R., Barnes, J. D., Sharp, Z. D., et al. (2015). Temporal variations in fumarole gas chemistry at Poas volcano, Costa Rica. *Journal of Volcanology and Geothermal Research*, *294*, 56–70.

Fischer, T. P., Shaw, A. M., & Hilton , D. R. (2007). Gas geochemistry of volcanic and hydrothermal fluids of Central America. In J. Bundschuh, & G. E. Alvarado (Eds.), *Central America: Geology, resources and hazards* (Vol. 2, pp. 839–867), Leiden, The Netherlands: Taylor and Francis.

Fischer, T. P., Takahata, N., Sano, Y., Sumino, H., & Hilton, D. R. (2005). Nitrogen isotopes of the mantle: Insights from mineral separates. *Geophysical Research Letters*, *32*, L11305. https://doi.org/10.1029/2005GL022792

Freundt, A., Grevemeyer, I., Rabbel, W., Hensen, C., Wehrmann, H., Kutterolf, S., et al. (2014). Volatile (H_2O, CO_2, Cl, S) budget of the Central American subduction zone. *International Journal of Earth Sciences*, *103*(7), 2101. https://doi.org/10.1007/s00531-014-1001-1

Gennaro, M. E., Grassa, F., Martelli, M., Renzulli, A., & Rizzo, A. L. (2017). Carbon isotope composition of CO_2-rich inclusions in cumulate-forming mantle minerals from Stromboli volcano (Italy). *Journal of Volcanology and Geothermal Research*, *346*, 95–103. http://dx.doi.org/10.1016/j.jvolgeores.2017.04.001

Global Volcanism Program (2002). Report on Pacaya (Guatemala). In R. Wunderman (Ed.), *Bulletin of the global volcanism network* (27:7). Smithsonian Institution. https://doi.org/10.5479/si.GVP.BGVN200207-342110

Goff, F., McMurtry, G. M., Counce, D., Simac, J. A., Roldan-Manzo, A. R., & Hilton, D. R. (2000). Contrasting hydrothermal activity at Sierra Negra and Alcedo volcanoes, Galapagos Archipelago, Ecuador. *Bulletin of Volcanology*, *62*(1), 34–52.

Graham, D. W. (2002). Noble gas isotope geochemistry of Mid-Ocean Ridge and Ocean Island Basalts: Characterization of mantle source reservoirs. In Porcelli, D., Ballentine, C. J., & Wieler, R. (Eds.), *Reviews in mineralogy and geochemistry, Volume 47: Noble gases in geochemistry and cosmochemistry* (pp. 245–317). Washington, DC: The Mineralogical Society of America.

Granieri, D., Salerno, G., Liuzzo, M., La Spina, A., Giuffrida, G., Caltabiano, T., et al. (2015). Emission of gas and atmospheric dispersion of SO_2 during the December 2013 eruption at San Miguel volcano (El Salvador, Central America). *Geophysical Research Letters*, *42*, 5847–5854. https://doi.org/10.1002/2015GL064660

Heydolph, K., Hoernle, K., Hauff, F., Den Bogaard, P. V., Portnyagin, M., Bindeman, I., & Garbe-Schönberg, D. (2012). Along and across arc geochemical variations in NW Central America: Evidence for involvement of lithospheric pyroxenite. *Geochimica et Cosmochimica Acta*, *84*, 459–491.

Hilton, D. R., Fischer, T. P., & Marty, B. (2002). Noble Gases and Volatile Recycling at Subduction Zones. *Reviews in Mineralogy & Geochemistry*, *47*(1), 319–370.

Hilton, D. R., Ramírez, C. J., Mora-Amador, R., Fischer, T. P., Füri, E., Barry, P. H., & Shaw, A. M. (2010). Monitoring of temporal and spatial variations in fumarole helium and carbon dioxide characteristics at Poás and Turrialba Volcanoes, Costa Rica (2001–2009). *Geochemical Journal*, *44*(5), 431–440.

Iacono-Marziano , G., Paonita, A., Rizzo, A., B., Scaillet, B., & Gaillard, F. (2010). Noble gas solubilities in silicate melts: New experimental results and a comprehensive model of the effects of liquid composition, temperature and pressure. *Chemical Geology*, *279*(3–4), 145–157. https://doi.org/10.1016/j.chemgeo.2010.10.017

INSIVUMEH. (2016). Volcàn Pacaya (monthly report 1402-11).

Janik, C. J., Goff, F., Fahlquist, L., Adams, A. I., Roldan, A., Chipera, S. J., et al. (1992). Hydrogeo- chemical exploration of geothermal prospects in the Tecuamburro Volcano region, Guatemala. *Geothermics*, *21*(4), 447–481.

Javoy, M., & Pineau, F. (1991). The volatiles record of a popping rock from the Mid-Atlantic ridge at 148N: Chemical and isotopic composition of a gas trapped in the vesicles. *Earth Planetary Science Letters*, *107*(3–4), 598–611.

Javoy, M., Pineau, F., & Iiyama, I. (1978). Experimental determination of the isotopic fractionation between gaseous CO_2 and carbon dissolved in tholeiitic magma: A preliminary study. *Contributions to Mineralogy and Petrology*, *67*(1), 35–39.

Kantzas, E. P., McGonigle, A. J. S., Tamburello, G., Aiuppa, A., & Bryant, R. G. (2010). Protocols for UV camera volcanic SO2 measurements. *Journal of Volcanology and Geothermal Research*, *194*(1–3), 55–60.

Kelemen , P. B., & Manning , C. E. (2015). Reevaluating carbon fluxes in subduction zones, what goes down, mostly comes up. *Proceedings of the National Academy of Sciences of the United States of America*, *112*(30), E3997. https://doi.org/10.1073/pnas.1507889112

Leeman, W. P., Carr, M. J., & Morris, J. D. (1994). Boron geochemistry of the Central American Volcanic Arc: Constraints on the genesis of subduction-related magmas. *Geochimica et Cosmochimca Acta*, *58*(1), 149–168.

Lucic, G., Stix, J., Sherwood Lollar, B., Lacrampe-Couloume, G., Muñoz, A., & Carcache, M. I. (2014). The degassing character of a young volcanic center: Cerro Negro, Nicaragua. *Bulletin of Volcanology*, *76*(9), 1–23.

Macpherson, C. G., & Mattey , D. P. (1994). Carbon isotope variations of CO_2 in LauBasin basalts and ferro basalts. *Earth and Planetary Science Letters*, *121*(3–4), 263–276.

Martin, R. S., Sawyer, G. M., Spampinato, L., Salerno, G. G., Ramirez, C., Ilyinskaya, E., et al. (2010). A total volatile inventory for Masaya Volcano, Nicaragua. *Journal of Geophysical Research*, *115*, B09215. https://doi.org/10.1029/2010JB007480

Marty, B. (2012). The origins and concentrations of water, carbon, nitrogen and noble gases on earth. *Earth and Planetary Science Letters*, *313–314*, 56–66.

Marty, B., & Jambon , A. (1987). C/3He fluxes from the solid Earth: Implications for carbon geodynamics. *Earth and Planetary Science Letters*, *83*(1–4), 16–26.

Mather, T. A., Pyle, D. M., Tsanev, V. I., McGonigle, A. J. S., Oppenheimer, C., & Allen, A. G. (2006). A reassessment of current volcanic emissions from the Central American arc with specific examples from Nicaragua. *Journal of Volcanology and Geothermal Research*, *149*(3–4), 297–311.

Matías Gómez, R. O., Rose, W. I., Palma, J. L., and Escobar-Wolf, R. (2012). *Notes on a map of the 1961–2010 eruptions of Volcán de Pacaya, Guatemala* (Digital Map Chart Ser. 10). Boulder, CO: Geological Society of America. https://doi.org/10.1130/2012.DMCH010

Matías Gómez, R. O., Rose, W. I., Palma, J. L., & Escobar-wolf, R. (2012), *Notes on a Map of the 1961 – 2010 Eruptions of Volcán de Pacaya, Guatemala* (Digital Map, pp. 1–10). Boulder, CO: Geological Society of America.

Mattey, D. P. (1991). Carbon dioxide solubility and carbon isotope fractionation in basaltic melt. *Geochimica et Cosmochimica Acta*, *55*(11), 3467–3473. https://doi.org/10.1016/0016-7037(91)90508-3

Morris, J. D., Leeman, W. P., & Tera, F. (1990). The subducted component in island arc lavas: Constraints from Be isotopes and B-Be systematics. *Nature*, *344*(6261), 31–36. https://doi.org/10.1038/344031a0

Moussallam, Y., Peters, N., Ramírez, C., Oppenheimer, C., Aiuppa, A., & Giudice, G. (2014). Characterization of the magmatic signature in gas emissions from Turrialba volcano, Costa Rica. *Solid Earth*, *6*(2), 2293–2320.

Noll , P. D., Jr., Newsom, H. E., Leeman, W. P., & Ryan, J. G. (1996). The role of hydrothermal fluids in the production of subduction zone magmas: Evidence from siderophile and chalcophile trace elements and boron. *Geochimica et Cosmochimica Acta* , *60*(4), 587–611.

Oppenheimer, C., Fischer, T. P., & Scaillet, B. (2014). Volcanic degassing: Process and impact. In H. D. Holland & K. K. Turekian (Eds.), *Treatise on geochemistry, The crust* (2nd ed., pp. 111–179). Amsterdam, Netherlands: Elsevier.

Ozima, M., & Podosek, F. A. (1983). *Noble gas geochemistry* (340. pp.). New York, NY: Cambridge University Press.

Patino, L. C., Carr, M. J., & Feigenson, M. D. (2000). Local and regional variations in Central American arc lavas controlled by variations in subducted sediment input. *Contributions to Mineralogy and Petrology*, *138*(3), 265–283.

Peccerillo, A., & Taylor, S. R. (1976). Rare earth elements in East Carpathian volcanic rocks. *Earth and Planetary Science Letters*, *32*(2), 121–126. https://doi.org/10.1016/0012-821X(76)90050-9

Poreda, R. J., & Craig, H. (1989). Helium isotope ratios in circum-Pacific volcanic arcs. *Nature* , *338*(6215), 473–478.

Rizzo, A. L., Barberi, F., Carapezza, M. L., Di Piazza, A., Francalanci, L., Sortino, F., et al. (2015). New mafic magma refilling a quiescent volcano: Evidence from He-Ne-Ar isotopes during the 2011–2012 unrest at Santorini, Greece. *Geochemistry, Geophysics, Geosystems*, *16*, 798–814. https://doi.org/10.1002/2014GC005653

Robidoux, P., Aiuppa, A., Rotolo, S. G., Rizzo, A. L., Hauri, E. H., & Frezzotti, M. L. (2017). Volatile contents of mafic-to-intermediate magmas at San Cristóbal volcano in Nicaragua. *Lithos*, *272–273*, 147–163. https://doi.org/10.1016/j.lithos.2016.12.002

Rodríguez, L., Watson, I. M., Rose, W. I., Branan, Y. K., Bluth, G. J. S., Chigna, G., et al. (2004). SO2 emissions to the atmosphere from active volcanoes in Guatemala and El Salvador, 1999–2002. *Journal of Volcanology and Geothermal Research*, *138*(3–4), 325–344.

Roggensack, K. (2001). Unraveling the 1974 eruption of Fuego volcano (Guatemala) with small crystals and their young melt inclusions. *Geology*, *29*(10), 911–914. https://doi.org/10.1130/0091-7613(2001)029<0911:UTEOFV>2.0.CO;2

Rose, W. I., Palma, J. L., Escobar Wolf, R., & Matías Gomez, R. O. (2013). A 50 yr eruption of a basaltic composite cone: Pacaya, Guatemala. In W. I. Rose, J. L. Palma, H. Delgado Granados, & N. Varley (Eds.), Understanding open-vent volcanism and related hazards: (Special Paper 498, p. 1–21). Boulder, CO: Geological Society of America. https://doi.org/10.1130/2013.2498(01)

Sadofsky, S. J., Portnyagin, M., Hoernle, K., & van den Bogaard, P. (2008). Subduction cycling of volatiles and trace elements through the Central American volcanic arc: Evidence from melt inclusions. *Contributions to Mineralogy and Petrology*, *155*(4), 433–456.

Salters , V. J. M., & Stracke, A. (2004). Composition of the depleted mantle. *Geochemistry, Geophysics, Geosystems*, *5*, Q05B07. https://doi.org/10.1029/2003GC000597

Sano, Y., & Marty , B. (1995). Origin of carbon in fumarolic gas from island arcs. *Chemical Geology*, *119*(1–4), 265–274.

Sano, Y., & Williams, S. N. (1996). Fluxes of mantle and subducted carbon along convergent plate boundaries. *Geophysical Research Letters*, *23*(20), 2749–2752.

Sano, Y., & Wakita, H. (1985). Geographical distribution of 3He/4He ratios in Japan: Implications for arc tectonics and incipientmagmatism. *Journal of Geophysical Research: Solid Earth*, *90*, 8729–8741. http://dx.doi.org/10.1029/JB090iB10p08729

Schaefer, L. N., Oommen, T., Corazzato, C., Tibaldi, A., & Rose, W. I. (2012), Numerical modeling of volcanic slope instability and related hazards at Pacaya Volcano, Guatemala. In *46th US Rock Mechanics. Geomechanics Symposium 2012* (Vol. 4, pp. 2844–2851). Berlin Heidelberg: Springer.

Shaw, A. M., Hilton, D. R., Fischer, T. P., Walker, J. A., & Alvarado, G. E. (2003). Contrasting He-C relationships in Nicaragua and Costa Rica: Insights into C cycling through subduction zones. *Earth and Planetary Science Letters*, *214*(3–4), 499–513.

Shaw, A. M., Hilton, D. R., Fischer, T. P., Walker, J. A., & de Leeuw, G. A. M. (2006). Helium isotope variations in mineral separates from Costa Rica and Nicaragua: Assessing crustal contributions, timescale variations and diffusion-related mechanisms. *Chemical Geology*, *230*(1–2), 124–139.

Shinohara, H. (2005). A new technique to estimate volcanic gas composition: Plume measurements with a portable multi-sensor system. *Journal of Volcanology and Geothermal Research*, *143*(4), 319–333.

Shinohara, H., Aiuppa, A., Giudice, G., Gurrieri, S., & Liuzzo, M. (2008). Variation of H_2O/CO_2 and CO_2/SO_2 ratios of volcanic gases discharged by continuous degassing of Mount Etna volcano, Italy. *Journal of Geophysical Research*, *113*, B09203. https://doi.org/10.1029/2007JB005185

Snyder, G., Poreda, R., Hunt, A. G., & Fehn, U. (2001). Regional variations in volatile composition: Isotopic evidence for carbonate recycling in the Central American volcanic arc. *Geochemistry, Geophysics, Geosystems*, *2*(10), 1057. https://doi.org/10.1029/2001GC000163

Symonds, R. B., Gerlach , T. M., & Reed, M. H. (2001). Magmatic gas scrubbing: Implications for volcano monitoring. *Journal of Volcanology and Geothermal Research*, *108*(1–4), 303–341.

Symonds, R. B., Rose, W. I., Bluth, G. J. S., & Gerlach, T. M. (1994). Volcanic-gas studies: Methods, results and applications. *Reviews in Mineralogy*, *30*, 1–66.

Syracuse, E. M., & Abers, G. A. (2006). Global compilation of variations in slab depth beneath arc volcanoes and implications. *Geochemistry, Geophysics, Geosystems*, *7*, Q05017. https://doi.org/10.1029/2005GC001045

Tamburello, G. (2015). Ratiocalc: Software for processing data from multicomponent volcanic gas analyzers. *Computers & Geoscience*, *82*, 63–67.

Tamburello, G., Aiuppa, A., Kantzas, E. P., McGonigle, A. J. S., & Ripepe, M. (2012). Passive vs. active degassing modes at an open-vent volcano (Stromboli, Italy). *Earth and Planetary Science Letters*, *359–360*, 106–116.

Tamburello, G., Kantzas, E. P., McGonigle, A. J. S., Aiuppa, A., & Giudice, G. (2011). UV camera measurements of fumarole field degassing (La Fossa crater, Vulcano Island). *Journal of Volcanology and Geothermal Research*, *199*(1–2), 47–52.

Tassi, F., Vaselli, O., Barboza, V., Fernandez, E., & Duarte, E. (2004). Fluid geochemistry and seismic activity in the period 1998–2002 at Turrialba Volcano (Costa Rica). *Annals of Geophysics*, *47*, 1501–1511.

Trull, T., Nadeau, S., Pineau, F., Polve, M., & Javoy, M. (1993). C–He systematics in hotspot xenoliths: Implications for mantle carbon contents and carbon recycling. *Earth and Planetary Science Letters*, *118*(1–4), 43–64.

Vaselli, O., Tassi, F., Duarte, E., Fernandez, E., Poreda, R. J., & Huertas, A. D. (2010). Evolution of fluid geochemistry at the Turrialba volcano (Costa Rica) from 1998 to 2008. *Bulletin of Volcanology*, *72*(4), 397–410.

Walker, J. A., Mickelson, J. E., Thomas, R. B., Patino, L. C., Cameron, B., Carr, M. J., et al. (2007). U-series disequilibria in Guatemalan lavas, crustal contamination, and implications for magma genesis along the Central American subduction zone. *Journal of Geophysical Research*, *112*, B06205. https://doi.org/10.1029/2006JB004589

Walker, J. A., Patino, L. C., Carr , M. J., & Feigenson, M. D. (2001). Slab control over HFSE depletions in central Nicaragua. *Earth and Planetary Science.Letters*, *192*(4), 533–543.

Walker, J. A., Roggensack, K., Patino, L. C., Cameron, B. I., & Matías, O. (2003). The water and trace element contents of melt inclusions across an active subduction zone. *Contributions to Mineralogy and Petrology*, *146*(1), 62–77.

Walker, J. A., Teipel, A. P., Ryan, J. G., & Syracuse , E. (2009). Light elements and Li isotopes across the northern portion of the Central American subduction zone. *Geochemistry, Geophysics, Geosystems*, *10*, Q06S16. https://doi.org/10.1029/2009GC002414

Wallace, P. J. (2005). Volatiles in subduction zone magmas: Concentrations and fluxes based on melt inclusion and volcanic gas data. *Journal of Volcanology and Geothermal Research*, *140*(1–3), 217–240.

Wallace, P. J., Plank, T., Edmonds, M., & Hauri, E. H. (2015). Volatiles in magmas. In H. Sigurdsson, B. Houghton, S. McNutt, H. Rymer, & J. Stix (Eds.), *The encyclopedia of volcanoes* (2nd ed., pp. 163–183). San Diego, CL: Elsevier Inc., Academic Press.

Wardman, J.; Sword-Daniels, V.; Stewart, C. & Wilson, T. (2012). Impact assessment of the May 2010 eruption of Pacaya volcano, Guatemala. *GNS Science Report*, *2012/09*, 90.

Wehrmann, H., Hoernle, K., Portnyagin, M., Wiedenbeck, M., & Heydolph, K. (2011). Volcanic CO_2 output at the Central American subduction zone inferred from melt inclusions in olivine crystals from mafic tephras. *Geochemistry, Geophysics, Geosystems*, *12*, Q06003. https://doi.org/10.1029/2010GC003412

Wunderman, R. L., & Rose, W. I. (1984). Amatitlán, an actively resurging caldera 10 km south of Guatemala City. *Journal of Geophysical Research*, *89(B10)*, 8525–8539.